This article has been accepted for publication in IEEE Transactions on Power Delivery. This is the author's version which has not been fully edited and content may change prior to final publication. Citation information: DOI 10.1109/TPWRD.2022.3195075



# AMI Data-driven Strategy for Hierarchical Estimation of Distribution Line Impedances

Jaepil Ban, *Member*, *IEEE*, Jae-Young Park, *Student Member*, *IEEE*, Young-Jin Kim, *Senior Member*, *IEEE*, and João P. S. Catalão, *Senior Member*, *IEEE*

***Abstract*—Monitoring, operation, and protection of distribution power grids fundamentally rely on the accurate estimation of line impedances. However, line impedance estimation is challenging due to the difficulties in modeling the dependence on line temperature and aging. This paper proposes a new data-driven strategy to estimate low-voltage (LV) and medium-voltage (MV) line impedances using an advanced metering infrastructure (AMI). In the proposed strategy, two-level optimization problems are formulated using generalized equations for voltage drops along LV and MV lines and then extended based on AMI data collected over time. Hierarchical estimation is achieved using the local and global references to the LV and MV root buses, respectively, enabling parallel estimation for individual LV grids and thus reduced computation time. Reinforcement learning is also integrated to compensate for possible measurement errors in the AMI data, ensuring robust estimation of LV and MV line impedances. The proposed strategy is tested on a three-phase unbalanced MV grid with multiple single-phase LV grids under various conditions characterized by measurement samples and errors. The results of case studies and sensitivity analyses confirm that the proposed strategy improves the accuracy and robustness of line impedance estimation at both LV and MV levels.**

***Index Terms*—advanced metering infrastructure, distribution power grids, line impedance estimation, reinforcement learning, two-level optimization problems.**

## NOMENCLATURE

***Sets***

| | |
|---|---|
| $s$ | index for Gauss-Newton iterations |
| $i, j, k$ | indices for medium voltage (MV) buses |
| $l, m, n$ | indices for low voltage (LV) buses |
| $L, M$ | subscripts for low- and medium-voltage grids |
| $\phi$ | superscript for phases $a$, $b$, and $c$ |
| $\lvert\bullet\rvert$, $\hat{\bullet}$, $\breve{\bullet}$ | absolute, estimated, and compensated values of $\bullet$ |
| $\tilde{\bullet}$ | augmented vector of $\bullet$ for multiple data samples |
| $\overline{\bullet}$, $\underline{\bullet}$ | maximum and minimum values of $\bullet$ |
| $\bar{\bullet}$ | target network of neural network $\bullet$ |
| $\mathcal{E}_M$ | set of lines connecting two MV buses |
| $\mathcal{E}^{\phi}_{Li}$ | set of lines connecting two LV buses in $\mathcal{SN}(i, \phi)$ |
| $\mathcal{IE}^{\phi}_i$, $\mathcal{IN}^{\phi}_i$ | sets of internal lines and buses in $\mathcal{SN}(i, \phi)$ |
| $\mathcal{LE}^{\phi}_i$ | set of lines between internal and end buses in $\mathcal{SN}(i, \phi)$ |
| $\mathcal{LE}^{\phi}_{i,m}$ | set of all pairs of lines directly connecting internal bus $m$ to two end buses in $\mathcal{SN}(i, \phi)$ |
| $\mathcal{LN}^{\phi}_i$ | set of end buses in $\mathcal{SN}(i, \phi)$ |
| $\mathcal{N}_M$, $\mathcal{N}^{\phi}_{Li}$ | sets of MV buses and LV buses in $\mathcal{SN}(i, \phi)$ |
| $\mathcal{P}_i$, $\mathcal{P}_{ij}$ | sets of phases for bus $i \in \mathcal{N}_M$ and line $(i, j) \in \mathcal{E}_M$ |
| $\mathcal{SN}(i, \phi)$ | LV grid connected to MV bus $i$ with phase $\phi$ |

***Scalars, vectors, and matrices***

| | |
|---|---|
| $\alpha$ | coefficient to update policy and Q target networks |
| $\lambda$ | penalty factor for $l_1$-norm regularization |
| $\mu$ | scale factor for Geman-McClure loss function |
| $\nu$ | exploration noise for reinforcement learning (RL) |
| $t^{\phi(s)}_i$ | step size of $s_{\text{th}}$ Gauss-Newton iteration for $\mathcal{SN}(i, \phi)$ |
| $\upsilon^{\phi}_i$, $w^{\phi}_i$ | Q function and Q network to compensate for errors in the measurements collected from $\mathcal{SN}(i, \phi)$ |
| $\varepsilon$ | threshold to stop Gauss-Newton iterations |
| $\varphi^{\phi}_{Li,m}$ | power factor angle at LV bus $m$ in $\mathcal{SN}(i, \phi)$ |
| $\boldsymbol{\zeta}^{\phi}_i$, $\boldsymbol{\xi}^{\phi}_i$ | weights of policy and Q networks for $\mathcal{SN}(i, \phi)$ |
| $I^{\phi}_{Li,m\text{-}n}$, $I^{\phi}_{M,i\text{-}j}$ | currents flowing through LV line $(m, n) \in \mathcal{E}^{\phi}_{Li}$ and MV line $(i, j) \in \mathcal{E}_M$ with phase $\phi \in \mathcal{P}_{ij}$ |
| $I^{\phi}_{M,i}$, $J^{\phi}_{M,i}$ | current flowing into MV bus $i \in \mathcal{N}_M$ with phase $\phi \in \mathcal{P}_i$ based on global and local voltage angle references |
| $IN^{\phi}_i$ | total number of downstream buses for each LV bus in $\mathcal{SN}(i, \phi)$: i.e., $IN^{\phi}_{Li} \coloneqq \sum_{m \in \mathcal{N}^{\phi}_{Li}} \lvert\mathcal{IN}^{\phi}_{Li,m}\rvert$ |
| $K$ | number of measurement dataset samples |
| $l$ | $L_2$ loss function to train Q network |
| $N_\pi$, $N_Q$ | numbers of hidden nodes in policy and Q networks |
| $N_M$ | number of MV buses |
| $RN^{\phi}_i$ | number of LV buses directly connected to the root bus in $\mathcal{SN}(i, \phi)$ |
| $V^{\phi}_{Li,m}$ | voltage at LV bus $m$ in $\mathcal{SN}(i, \phi)$ |
| $V^{\phi}_{M,i}$, $U^{\phi}_{M,i}$ | voltage at MV bus $i$ with phase $\phi \in \mathcal{P}_i$ based on global and local voltage angle references |
| $Z^{\phi}_{Li,m\text{-}n}$ | impedance of line $(m, n) \in \mathcal{E}^{\phi}_{Li}$ |
| $\mathbf{a}^{\phi}_i$, $r^{\phi}_i$ | action and reward of the RL agent for $\mathcal{SN}(i, \phi)$ |
| $\mathbf{e}_{i,m}$ | measurement error at LV bus $m$ |
| $\mathbf{f}^{\phi}_i$, $\mathbf{F}^{\phi}_i$, $\mathbf{g}$, $\mathbf{G}$ | objective functions of impedance estimation problems |
| $\mathbf{o}^{\phi}_i$, $\mathbf{o}^{\phi}_{i,(p)}$ | measurement dataset and $p_{\text{th}}$ sample for $\mathcal{SN}(i, \phi)$ |
| $\mathbf{u}$ | virtual measurement dataset at MV buses |
| $\mathbf{x}^{\phi}_i$, $\mathbf{y}$ | decision variables for impedance estimation problems |
| $\boldsymbol{\pi}^{\phi}_i$ | learning policy for $\mathcal{SN}(i, \phi)$ |
| $\mathcal{J}^{\phi}_i$ | Jacobian matrix of $\mathbf{F}^{\phi}_i(\cdot)$ |
| $\mathbf{R}^{\phi}_{Li}$, $\mathbf{X}^{\phi}_{Li}$, $\Delta\boldsymbol{\theta}^{\phi}_{Li}$ | line resistance, line reactance, and voltage angle for $\mathcal{SN}(i, \phi)$ |
| $\Delta\mathbf{R}^{\phi}_{Li}$, $\Delta\mathbf{X}^{\phi}_{Li}$, $\Delta\lvert\mathbf{V}^{\phi}_{Li}\rvert$ | incremental adjustments to the estimates of line resistance, line reactance, and bus voltage magnitudes |
| $\mathbf{V}_{M,i}$, $\mathbf{I}_{M,i\text{-}j}$, | voltage vector at MV bus $i \in \mathcal{N}_{MV}$ and current vector flowing through MV line $(i, j) \in \mathcal{E}_{MV}$ |
| $\mathbf{R}_{M,i\text{-}j}$, $\mathbf{X}_{M,i\text{-}j}$, $\mathbf{Z}_{M,i\text{-}j}$ | resistance, reactance, and impedance of line $(i, j) \in \mathcal{E}_M$ |

## I. INTRODUCTION

ACCURATE and robust estimation of distribution line impedances is of key importance in improving the

Manuscript received February 08, 2022. This work was supported by the National Research Foundation of Korea(NRF) grant Funded by the Korea government(MSIT) under Grant 2019R1C1C1003361. *(Corresponding author: Y. Kim)*

J. Ban is with the School of Electronic Engineering, Kumoh National Institute of Technology, Gumi, Gyeongbuk 39177 South Korea.

J. Park is with the Korea Institute of Energy Research (KIER), Daejeon 34129 South Korea.

Y. Kim are with the Department of Electrical Engineering, Pohang University of Science and Technology (POSTECH), Pohang, Gyeongbuk 37673 South Korea (powersys@postech.ac.kr).

J. P. S. Catalão is with the Faculty of Engineering of the University of Porto, and also with INESC TEC, 4200-465 Porto, Portugal.

© 2022 IEEE. Personal use is permitted, but republication/redistribution requires IEEE permission. See https://www.ieee.org/publications/rights/index.html for more information.
Authorized licensed use limited to: b-on: UNIVERSIDADE DO PORTO. Downloaded on August 07,2022 at 15:07:28 UTC from IEEE Xplore. Restrictions apply.

This article has been accepted for publication in IEEE Transactions on Power Delivery. This is the author's version which has not been fully edited and content may change prior to final publication. Citation information: DOI 10.1109/TPWRD.2022.3195075



performance of functions required for grid operation, monitoring, and protection [1], [2], such as Volt/Var control, state estimation, and protection relay setting and coordination. In particular, line impedance estimation (LIE) directly affects the parameter settings of protection relays. This implies that accurate LIE is essential to improve the relay capability of detecting and locating a fault on a distribution power line with respect to the operating speed, accuracy, and reliability [3], [4]. It was reported in [5] that the uncertainty in line impedance estimates increases the tripping decision time of a relaying scheme. In practice, however, LIE remains challenging, for example, due to the difficulties in measuring line lengths and modeling time-varying dependence on line temperature and age [6], [7]. This leads to a large discrepancy between the designed and real-world performances of such functions, preventing the realization of smart distribution grids.

Meanwhile, micro phasor measurement units ($\mu$PMUs) and an advanced metering infrastructure (AMI) continue to be developed and deployed throughout distribution grids, providing unprecedented opportunities to electric utilities and distribution system operators for data-driven LIE, as listed in Table I. For example, in [8] and [9], frameworks for LIE using $\mu$PMU data were discussed based on an assumption that there were $\mu$PMUs at every bus in a distribution grid. In [10] and [11], $\mu$PMU data were used with AMI data to estimate the line impedances via an alternating direction method of multipliers (ADMM) and a nonparametric Kernel density approach, respectively. The underlying algorithms implemented in the frameworks mainly relied on the ability of $\mu$PMUs to measure both the magnitudes and angles of bus voltages and line currents. However, the costs of such measurement devices and their installation costs are high, limiting the applicability of these frameworks in practice. Recently, AMI has become a good alternative. It has been, and is currently being, installed at a number of customers' premises for various applications, such as monitoring building electricity use, real-time control of distributed energy resources (DERs), and optimal planning of grid reinforcement [12], [13].

In recent studies, AMI has been widely used for data-driven LIE at various voltage levels. For example, in [14], a regression method was implemented that adopted power-flow modeling to estimate line impedances at the medium-voltage (MV) level based on measurements of voltage magnitudes and power injections at MV buses. In [15]–[17], AMI data were collected from individual customer's premises to estimate low-voltage (LV) line impedances. However, in [14]–[17], the AMI-based LIE was achieved only for either an MV grid or an LV grid, rather than for both types of interconnected grids. Moreover, most of the studies focused on the estimation of three-phase balanced lines for simplicity, which is unlikely to be valid in real grids [18]. The limitations were mainly attributable to the nonlinear dependence of the voltage drop between two MV buses on the magnitudes and angles of all the line currents and all the bus voltages in the LV grids that are connected to each of the MV buses. The nonlinear dependence was commonly dealt with using an entire-circuit calculation method [19], rather than a hierarchical method. However, in the entire circuit method, voltage and current angles affect each other throughout all the MV and LV grids and, thus, angle calculation becomes computationally expensive, rendering AMI-based LIE in a three-phase unbalanced MV grid with multiple LV grids difficult.

For AMI-based LIE, an optimization problem needs to be formulated using nonlinear constraints on line voltage drops, because AMI can measure only the magnitudes of voltage, current, and power, unlike $\mu$PMUs. In most previous studies, the constraints were linearly approximated and, consequently, the optimal LIE problem was simplified to a linear least-squares (LLS) problem that could be readily solved using a common linear programming solver or even directly when the constraints were further relaxed. However, the linear approximation can lead to large errors in the LIE results, particularly, when the load demand in a distribution grid is high; hence, the voltage angle differences between neighboring buses cannot be neglected. Moreover, due to random measurement errors, the optimal LIE problem is inherently formulated in the form of an error-in-variable (EIV) problem, which is difficult to solve using a standard weighted least square (WLS) method. In [17], a particle swarm optimization (PSO) method was applied to solve the optimal LIE problem without linear approximation. However, every PSO iteration leads to a different solution due to the use of random mutation or random values. This requires a problem to be solved repeatedly to select the best local optimal

TABLE I. MEASUREMENTS, NETWORKS, PROBLEM FORMULATIONS AND SOLVERS, AND ERROR COMPENSATIONS OF DATA-DRIVEN LIE

| References | Measurements | Voltage levels | Network phases | Linear approximation errors | Solver | Data error compensation |
|---|---|---|---|---|---|---|
| Proposed | AMI | MV, LV | Unbalanced, multiple | - | Gauss-Newton | RL |
| [8] | PMU | MV | Single | - | Iterative WLS | - |
| [9] | PMU | MV | Balanced, multiple | - | EM | - |
| [10] | PMU, AMI | MV | Unbalanced, multiple | - | ADMM | - |
| [11] | PMU, AMI | LV | Single | - | QP | - |
| [14] | AMI | MV | Balanced, multiple | - | Newton-Raphson | - |
| [15] | AMI | LV | Unbalanced, multiple | O | Linear least square | LSF |
| [16] | AMI | LV | Unbalanced, multiple | O | Linear least square | LSF |
| [17] | PMU, AMI | LV | Single | - | PSO | - |
| [20] | AMI | LV | Single | - | TRR | LSF |

**EM**: expectation-maximization, **WLS**: weighted least squares, **LSF**: least square fitting, **TRR**: trust region reflective, **QP**: quadratic programming

© 2022 IEEE. Personal use is permitted, but republication/redistribution requires IEEE permission. See https://www.ieee.org/publications/rights/index.html for more information.
Authorized licensed use limited to: b-on: UNIVERSIDADE DO PORTO. Downloaded on August 07,2022 at 15:07:28 UTC from IEEE Xplore. Restrictions apply.

This article has been accepted for publication in IEEE Transactions on Power Delivery. This is the author's version which has not been fully edited and content may change prior to final publication. Citation information: DOI 10.1109/TPWRD.2022.3195075



estimates among those already obtained. The computation time eventually becomes significant, particularly for a large-scale grid with several unknown line impedances. To avoid the issue, deterministic nonlinear solvers were adopted in [14] and [20].

Although AMI technologies continue to evolve, the random measurement errors need to be addressed carefully; otherwise, AMI-based LIE performance can be compromised. Only a few studies have explicitly discussed measurement error compensation for an AMI-based LIE (e.g., [20]); however, the method discussed in [20] is applicable only when voltage magnitude and power injection are measured at all buses. The measurement errors can be successfully mitigated with reinforcement learning (RL). For example, in [21], RL was applied to update the estimates of the time-varying parameters of a solar panel, considering the measurement errors of its pyranometer. Moreover, in [22], RL was adopted to adjust the noise covariance matrix of an extended Kalman filter. [23] discusses the use of RL to determine the parameters of an active noise controller, reducing the effect of noise. However, further studies on the application of RL to measurement-error compensation in AMI data are still required, considering the number of impedance estimates that need to be explored and determined in a large, continuous action space.

This paper proposes a new AMI-based strategy to estimate line impedances in both LV and MV distribution grids. Hierarchical LIE is achieved by formulating and solving lower- and upper-level optimization problems. For each LV grid, a lower-level problem is established to estimate single-phase line impedances using the local reference to the LV root bus. This enables lower-level problems for individual LV grids to be solved in parallel. The upper-level problem is then updated to estimate the unbalanced line impedances in the MV grid for all phases. The variables affecting voltage angle differences between the MV and LV buses are also defined and integrated into the constraints on voltage drops along MV lines. This ensures accurate estimation of MV and LV line impedances based on the global reference to the MV root bus. To obtain reliable estimates, the optimal LIE problems are extended by considering AMI datasets collected over time and then solved using a deterministic Gauss-Newton (GN) algorithm. Moreover, in the proposed LIE strategy, an RL-based method is incorporated to compensate for measurement errors in the AMI data, enabling robust estimation of LV, and hence MV, line impedances. The results of case studies and sensitivity analyses confirm the good performance of the proposed strategy with regard to accuracy, robustness, and time efficiency.

The main contributions of this paper are summarized below:

- To the best of our knowledge, this is the first study to develop an AMI-based LIE strategy for a three-phase unbalanced MV grid with multiple single-phase LV grids.
- For AMI-based LIE, hierarchical optimization problems are established using local references to voltage angles and then further extended considering time-series datasets, enabling the problems to be reliably solved in parallel.
- The optimization problems are formulated directly using time-series AMI data and generalized, nonlinear voltage drop equations, thereby enabling the improvement of the LIE accuracy and the wide applications to distribution networks under various conditions characterized by network sizes, line configurations, load demands, and renewable generation.
- An RL-based method is developed to compensate for measurement errors in the AMI data and integrated with the hierarchical problems, enabling robust impedance estimation.

## II. Fundamentals

Fig. 1 shows the common structures and interconnections of radial distribution grids at the MV and LV levels. In the United States, MV levels range from 2.4 to 69 kV, and LV levels are below 1 kV [24]. Note that the proposed LIE strategy can be applied to different voltage levels, because it adopts per unit values. The MV can consist of single-, double-, or three-phase unbalanced lines, while the LV grids are single-phase lines. Each LV grid is connected to an MV bus via a single-phase transformer. In other words, MV buses and the corresponding LV root buses are located at the primary and secondary sides of single-phase two-winging transformers, respectively, based on [6], [7], and [16]. Note that the transformer connection also can be used to model different types of transformers, such as split, two, and three phases [15] and, hence, this implies that the proposed LIE strategy can be applied to LV grids with various line configurations. Moreover, in practice, manufacturers can often provide transformer impedances obtained using short- and open-circuit tests [25], [26], and this paper then focuses on estimating line impedances. When the impedances are not provided or incorrectly provided, they can be first estimated using the methods discussed in [27] and [28], for example, and then incorporated into the proposed LIE strategy; this is not further discussed here for brevity. In an LV grid, measurements of $|V|$, $P$, and $Q$ values at end buses (i.e., customers' premises) are collected by AMI and delivered via communication links to a distribution management system located in the MV grid [19].

Given the grid structures and interconnections, voltage drops along the MV line $(i, j) \in \mathcal{E}_M$ and the corresponding LV line $(m, n) \in \mathcal{E}^{\phi}_{Li}$ can be determined using generalized, nonlinear equations in phasor domain, respectively, as:

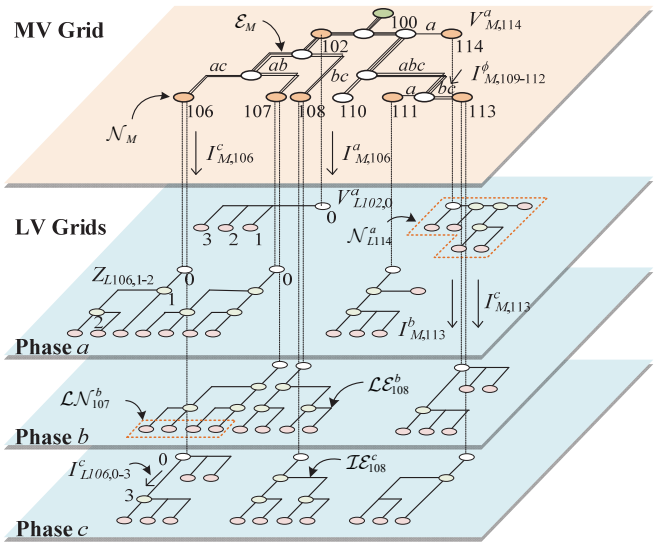


Fig. 1. An MV grid with single-, double-, or three-phase unbalanced lines where an MV bus is connected to multiple single-phase LV grids.

© 2022 IEEE. Personal use is permitted, but republication/redistribution requires IEEE permission. See https://www.ieee.org/publications/rights/index.html for more information.
Authorized licensed use limited to: b-on: UNIVERSIDADE DO PORTO. Downloaded on August 07,2022 at 15:07:28 UTC from IEEE Xplore. Restrictions apply.

This article has been accepted for publication in IEEE Transactions on Power Delivery. This is the author's version which has not been fully edited and content may change prior to final publication. Citation information: DOI 10.1109/TPWRD.2022.3195075



$$\mathbf{V}_{M,i} - \mathbf{V}_{M,j} - \mathbf{Z}_{M,i\text{-}j}\mathbf{I}_{M,i\text{-}j} = 0, \quad \forall (i,j) \in \mathcal{E}_M, \tag{1}$$

$$\text{and} \quad V^{\phi}_{Li,m} - V^{\phi}_{Li,n} = Z^{\phi}_{Li,m\text{-}n} I^{\phi}_{Li,m\text{-}n}, \quad \forall (m,n) \in \mathcal{E}^{\phi}_{Li}, \tag{2}$$

where $\mathbf{V}_{M,i}$ is the single-, double-, or three-phase voltage at MV bus $i$ and $\mathbf{I}_{M,i\text{-}j}$ is the single-, double-, or three-phase current flowing through line $(i, j) \in \mathcal{E}_M$. Similarly, $V^{\phi}_{Li,m}$ and $I^{\phi}_{Li,m\text{-}n}$ are the voltage at LV bus $m$ for phase $\phi$ and the current flowing through line $(m, n) \in \mathcal{E}^{\phi}_{Li}$, respectively. Note that (1) and (2) are nonlinear, because $\mathbf{V}_{M,i}$, $\mathbf{V}_{M,j}$, $\mathbf{I}_{M,i\text{-}j}$, $V^{\phi}_{Li,m}$, $V^{\phi}_{Li,n}$, and $I^{\phi}_{Li,m\text{-}n}$ are all complex variables with unknown phase angles; for example, $V^{\phi}_{M,i} = |U^{\phi}_{M,i}|(\cos\Delta\theta^{\phi}_{M,i} + j{\cdot}\sin\Delta\theta^{\phi}_{M,i})$ where $\Delta\theta^{\phi}_{M,i}$ is unknown. In the proposed strategy, (1) and (2) are not linearly approximated, but are used directly to establish the constraints for the optimal LIE problems, as discussed in Section III. The accuracy of the solutions can then be improved by avoiding errors that result from linearization. Note that the errors are considerable particularly when the load demand in the MV and LV grids is high; hence, the differences between voltage angles at neighboring buses become large.

## III. Problem Formulation for Data-Driven Estimation

### A. Hierarchical Estimation of LV and MV Line Impedances

The proposed AMI-based LIE is achieved by considering the hierarchical structures and connections of the MV and LV grids, shown in Fig. 1. Specifically, using (1) and (2), two-level optimization problems are formulated and extended for AMI datasets collected over time. At the lower level, an LIE problem is established to estimate the line impedances in each LV grid, based on the local reference to the LV root bus. In other words, the voltage angles at all LV buses are locally referenced to the voltage angle at the LV root bus, rather than at the MV root bus. This implies that the LIE problems for LV grids are independent of each other and can be solved in a distributed manner, thus reducing computation time. Given the AMI data and the lower-level solutions, we estimate the voltage and current magnitudes and the power injections at the MV buses. The upper-level LIE problem is then implemented to estimate the unbalanced line impedances in the MV grid for all phases. The variables for the voltage angle differences between the MV and LV root buses are defined and integrated into the constraints on (1), so that all the estimates become globally referenced to the MV root bus.

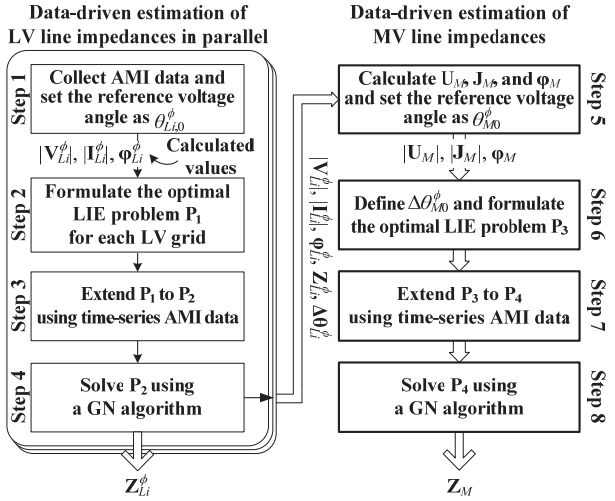


Fig. 2. Overall framework of the proposed estimation strategy.

Fig. 2 shows the overall framework of the proposed AMI-based LIE strategy, consisting primarily of eight steps. Briefly, Steps 1–4 describe the parallel LIE for individual LV grids, given the time-series AMI data of $|V^{\phi}_{Li,n}|$, $P^{\phi}_{Li,n}$, and $Q^{\phi}_{Li,n}$ and the corresponding calculated values of $|I^{\phi}_{Li,m\text{-}n}|$ and $\varphi^{\phi}_{Li,n}$ at the LV end buses. The solutions to the optimal LIE problems $\mathbf{P}_2$ for all the LV grids (i.e., the LV line impedance estimates) are then used as the virtual measurement data to formulate and solve the optimal LIE problem $\mathbf{P}_4$ for the MV grid. This corresponds to Steps 5–8.

### B. Estimation of LV Line Impedances

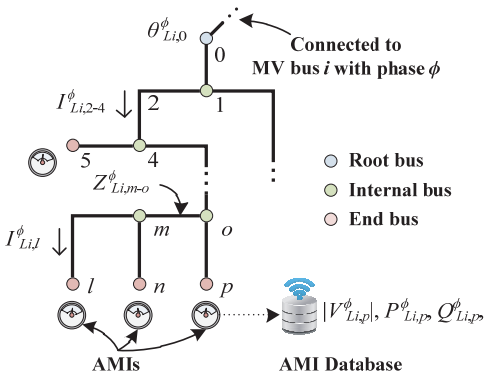


Fig. 3. Schematic diagram of LV grid $\mathcal{SN}(i, \phi)$ with root, internal, and end buses. AMI datasets of $|V^{\phi}_{Li}|$, $P^{\phi}_{Li}$, and $Q^{\phi}_{Li}$ are collected at LV end buses.

Fig. 3 shows a schematic diagram of the LV grid $\mathcal{SN}(i, \phi)$, where the AMI collects measurements of $|V^{\phi}_{Li,n}|$, $P^{\phi}_{Li,n}$, and $Q^{\phi}_{Li,n}$ at the end buses and calculates the corresponding $|I^{\phi}_{Li,m\text{-}n}|$ and $\varphi^{\phi}_{Li,n}$. For $\mathcal{SN}(i, \phi)$, the AMI-based LIE is then achieved by formulating and solving the unconstrained nonlinear optimization problem:

**$\mathbf{P}_1$: Line impedance estimation in LV grid $\mathcal{SN}(i, \phi)$**

$$\min_{\mathbf{x}^{\phi}_i} \| \mathbf{f}^{\phi}_i(\mathbf{x}^{\phi}_i, \mathbf{o}^{\phi}_i) \|_2^2, \tag{3}$$

$$\text{where} \quad \mathbf{f}^{\phi}_i(\mathbf{x}^{\phi}_i, \mathbf{o}^{\phi}_{Li}) = [\mathbf{f}^{\phi}_{i,1}{}^{\mathrm{T}}, \mathbf{f}^{\phi}_{i,2}{}^{\mathrm{T}}, \mathbf{f}^{\phi}_{i,3}{}^{\mathrm{T}}, \mathbf{f}^{\phi}_{i,4}{}^{\mathrm{T}}]^{\mathrm{T}}, \tag{4}$$

$$\mathbf{x}^{\phi}_i = [\mathbf{R}^{\phi}_{Li}{}^{\mathrm{T}}, \mathbf{X}^{\phi}_{Li}{}^{\mathrm{T}}, \boldsymbol{\Delta\theta}^{\phi}_{Li}{}^{\mathrm{T}}]^{\mathrm{T}}, \tag{5}$$

$$\mathbf{o}^{\phi}_i = [|\mathbf{V}^{\phi}_{Li}|^{\mathrm{T}}, |\mathbf{I}^{\phi}_{Li}|^{\mathrm{T}}, \boldsymbol{\varphi}^{\phi}_{Li}{}^{\mathrm{T}}]^{\mathrm{T}}. \tag{6}$$

In (3) and (4), $\mathbf{f}^{\phi}_{i,1}$ and $\mathbf{f}^{\phi}_{i,2}$ represent the real and imaginary parts of (2), respectively, for the lines between an internal bus and its end buses. Similarly, $\mathbf{f}^{\phi}_{i,3}$ and $\mathbf{f}^{\phi}_{i,4}$ correspond to the real and imaginary parts of (2) for the line between two neighboring buses. The detailed expressions are provided in Appendix A; see (A6)–(A9). In (3) and (5), $\mathbf{x}^{\phi}_i$ is the optimal estimate of $R^{\phi}_{Li,m\text{-}n}$, $X^{\phi}_{Li,m\text{-}n}$, and $\Delta\theta^{\phi}_{Li,n}$ (i.e., the LIE results), based on the local reference to the LV root bus. In other words, $\mathbf{x}^{\phi}_i$ is set as the decision variable vector for $\mathbf{P}_1$ and determined so that it minimizes the squared $L_2$-norm of $\mathbf{f}^{\phi}_i(\cdot)$, given the datasets of $\mathbf{o}^{\phi}_i$ measured and calculated by the AMI [see (6)].

In this paper, $\mathbf{P}_1$ is extended to $\mathbf{P}_2$ using a number of AMI datasets sampled over time, so that the reliability is improved in obtaining the optimal $\mathbf{x}^{\phi}_i$, as:

© 2022 IEEE. Personal use is permitted, but republication/redistribution requires IEEE permission. See https://www.ieee.org/publications/rights/index.html for more information.
Authorized licensed use limited to: b-on: UNIVERSIDADE DO PORTO. Downloaded on August 07,2022 at 15:07:28 UTC from IEEE Xplore. Restrictions apply.

This article has been accepted for publication in IEEE Transactions on Power Delivery. This is the author's version which has not been fully edited and content may change prior to final publication. Citation information: DOI 10.1109/TPWRD.2022.3195075



**$\mathbf{P}_2$: Extension of $\mathbf{P}_1$ using time-series AMI data**

$$\min_{\tilde{\mathbf{x}}_i^{\phi}} \| \mathbf{F}_i^{\phi}(\tilde{\mathbf{x}}_i^{\phi}, \tilde{\mathbf{o}}_i^{\phi}) \|_2^2 , \tag{7}$$

where $\mathbf{F}_i^{\phi}(\cdot) \coloneqq [\mathbf{f}_i^{\phi}(\cdot, \mathbf{o}_{i,(1)}^{\phi})^{\mathrm{T}}, \mathbf{f}_i^{\phi}(\cdot, \mathbf{o}_{i,(2)}^{\phi})^{\mathrm{T}}, \ldots, \mathbf{f}_i^{\phi}(\cdot, \mathbf{o}_{i,(K)}^{\phi})^{\mathrm{T}}]^{\mathrm{T}}$, (8)

$$\tilde{\mathbf{x}}_i^{\phi} \coloneqq [\mathbf{R}_{Li}^{\phi\mathrm{T}}, \mathbf{X}_{Li}^{\phi\mathrm{T}}, \Delta\tilde{\boldsymbol{\theta}}_{Li}^{\phi\mathrm{T}}]^{\mathrm{T}}, \tag{9}$$

$$\Delta\tilde{\boldsymbol{\theta}}_{Li}^{\phi} \coloneqq [(\Delta\boldsymbol{\theta}_{Li,(1)}^{\phi})^{\mathrm{T}}, (\Delta\boldsymbol{\theta}_{Li,(2)}^{\phi})^{\mathrm{T}}, \ldots (\Delta\boldsymbol{\theta}_{Li,(K)}^{\phi})^{\mathrm{T}}]^{\mathrm{T}}, \tag{10}$$

$$\tilde{\mathbf{o}}_i^{\phi} \coloneqq [(\mathbf{o}_{i,(1)}^{\phi})^{\mathrm{T}}, (\mathbf{o}_{i,(2)}^{\phi})^{\mathrm{T}}, \ldots (\mathbf{o}_{i,(K)}^{\phi})^{\mathrm{T}}]^{\mathrm{T}}, \tag{11}$$

(5), and (6).

In (8) and (9), $\mathbf{F}_i^{\phi}(\tilde{\mathbf{x}}_i^{\phi}, \tilde{\mathbf{o}}_i^{\phi})$ represents a set of $\mathbf{f}_i^{\phi}(\mathbf{x}_i^{\phi}, \mathbf{o}_i^{\phi})$ [see (4)] for all the time-series AMI datasets $\mathbf{o}_{i,(p)}^{\phi}$, and $\tilde{\mathbf{x}}_i^{\phi}$ is a set of corresponding decision variable vectors. In other words, $\mathbf{f}_i^{\phi}(\mathbf{x}_i^{\phi}, \mathbf{o}_i^{\phi})$ in $\mathbf{P}_1$ is extended to $\mathbf{F}_i^{\phi}(\tilde{\mathbf{x}}_i^{\phi}, \tilde{\mathbf{o}}_i^{\phi})$ in $\mathbf{P}_2$. Note that the decision variables $\mathbf{R}_{Li}^{\phi}$ and $\mathbf{X}_{Li}^{\phi}$ are shared in $\mathbf{f}_i^{\phi}(\mathbf{x}_i^{\phi}, \mathbf{o}_i^{\phi})$, because the line impedances do not vary within a short period of time. Moreover, in (10), $\Delta\tilde{\boldsymbol{\theta}}_{Li}^{\phi}$ is defined as a set of $\Delta\boldsymbol{\theta}_{Li,(p)}^{\phi}$ [see (5)] for all $p = 1, \cdots, K$, where $K$ is the total number of AMI datasets. Unlike the case of $\mathbf{R}_{Li}^{\phi}$ and $\mathbf{X}_{Li}^{\phi}$, $\Delta\boldsymbol{\theta}_{Li}^{\phi}$ varies over time and, consequently, the number of the decision variables $\Delta\tilde{\boldsymbol{\theta}}_{Li}^{\phi}$ in $\mathbf{P}_2$ increases with the number of the time-series AMI datasets.

The numbers of elements in $\mathbf{F}_i^{\phi}(\cdot)$ and $\tilde{\mathbf{x}}_i^{\phi}$ can be calculated, respectively, as:

$$(2 \times \binom{IN_i^{\phi}}{2} + |\mathcal{IE}_i^{\phi}|) \times K, \tag{12}$$

and $$2IN_i^{\phi} + (|\mathcal{LN}_i^{\phi}| - 1) \times K. \tag{13}$$

In other words, (12) and (13) represent the numbers of equations and decision variables, respectively, for the optimal LIE problem $\mathbf{P}_2$. It can be seen that as $K$ increases, the Jacobian matrix of $\mathbf{F}_i^{\phi}(\cdot)$ is more likely to become full rank and hence the solution of $\mathbf{P}_2$ can be reliably obtained for any topology of the LV grid $\mathcal{SN}(i, \phi)$. For example, a simple LV grid consists of one parent bus and three leaf buses, each of which is connected to the parent bus separately, leading to $IN_i^{\phi} = 3$, $|\mathcal{LN}_i^{\phi}| = 3$, and $|\mathcal{IE}_i^{\phi}| = 0$. Given $K$ AMI datasets, the number of the LIE equations is $6K$, considering the real and imaginary parts of (2) for each line. Meanwhile, the number of decision variables is $6+2K$, considering the estimates of resistance and reactance for each line and the estimates of phase angle differences among three leaf buses for each dataset. For the LV grid, $K \geq 2$ then should be satisfied to ensure that $\mathbf{P}_2$ has a feasible solution (i.e., $6K \geq 6 + 2K$). Note that considering the errors in the measurement datasets, a larger value of $K$ (i.e., more AMI datasets) improves the LIE accuracy, facilitating the practical application of AMI-based LIE, as discussed in Section IV-C.

To solve $\mathbf{P}_2$, a GN algorithm is adopted whereby the optimal estimates $\tilde{\mathbf{x}}_i^{\phi}$ are searched for by moving in the direction opposite to the gradient of $\mathbf{F}_i^{\phi}(\cdot)$, as:

$$\tilde{\mathbf{x}}_i^{\phi(s+1)} = \tilde{\mathbf{x}}_i^{\phi(s)} - t_i^{\phi(s)} \cdot \nabla_{\mathbf{x}}\mathbf{F}_i^{\phi}(s), \quad \text{and} \tag{14}$$

$$\nabla_{\mathbf{x}}\mathbf{F}_i^{\phi}(s) \coloneqq (\mathcal{J}_i^{\phi\mathrm{T}}\mathcal{J}_i^{\phi})^{-1}\mathcal{J}_i^{\phi\mathrm{T}}\mathbf{F}_i^{\phi}(\tilde{\mathbf{x}}_i^{\phi(s)}, \tilde{\mathbf{o}}_i^{\phi}). \tag{15}$$

As the GN iteration continues, the search step size $t_i^{\phi}$ is adaptively adjusted using a backtracking line search [29] to improve the convergence rate. The GN iteration stops when $\|\nabla_{\mathbf{x}}\mathbf{F}_i^{\phi}(\cdot)\|_2 < \varepsilon$. Note that the convergence of the GN algorithm is guaranteed under the condition that the initial values (i.e., at $s = 0$) of the decision variables are close to the actual values; please refer to Appendix C for details.

### *C. Estimation of MV Line Impedances for All Phases*

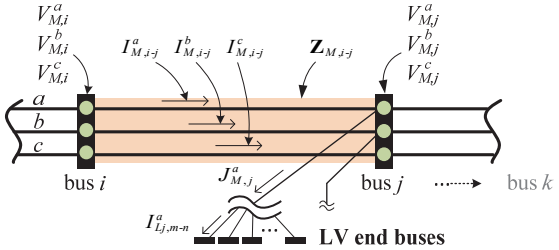


Fig. 4. Schematic diagram of MV buses $i$ and $j$ where LV grids $\mathcal{SN}(j, \phi)$ are connected.

Fig. 4 shows a schematic diagram of neighboring buses at the MV level, where single-phase LV grids $\mathcal{SN}(j, \phi)$ are connected to MV bus $j$ with phases $a$ and $b$, for example. To estimate $\mathbf{Z}_{M,i\text{-}j}$, the bus voltages, line currents, and power factor angles at all MV buses are first calculated using the AMI data and the $\mathbf{P}_2$ solutions for all the LV grids, as:

$$V_{M,i}^{\phi} = \left|U_{M,i}^{\phi}\right| \exp\left(j\Delta\theta_{M,i}^{\phi}\right), \tag{16}$$

$$I_{M,i\text{-}j}^{\phi} = \left|J_{M,j}^{\phi}\right| \exp\left(j\Delta\theta_{M,j}^{\phi} - j\varphi_{M,j}^{\phi}\right) + \sum\nolimits_{k:j\to k} I_{M,j\text{-}k}^{\phi}, \tag{17}$$

$$\varphi_{M,i}^{\phi} = \arg(U_{M,i}^{\phi} J_{M,i}^{\phi\,*}), \tag{18}$$

where $$U_{M,i}^{\phi} = \frac{1}{RN_i^{\phi}} \sum_{m:0\to m} \left\{V_{Li,m}^{\phi} + Z_{Li,0\text{-}m}^{\phi} I_{Li,0\text{-}m}^{\phi}\right\}, \tag{19}$$

$$J_{M,j}^{\phi} = \sum_{(m,n)\in\mathcal{LE}_i^{\phi}} \left|I_{Lj,m\text{-}n}^{\phi}\right| \exp\left(j\Delta\theta_{Li,n}^{\phi} - j\varphi_{Li,n}^{\phi}\right). \tag{20}$$

Specifically, for the hierarchical estimation, $\Delta\theta_{Li,n}^{\phi}$ in (20) are determined based on the local reference to the root bus in each LV grid, rather than the global reference to the MV root bus, as discussed in Section III-B. Consequently, the angles of $U_{M,i}^{\phi}$ and $J_{M,i\text{-}j}^{\phi}$ (i.e., $\theta_{M,i}^{\phi}$ and $\theta_{M,i}^{\phi} - \varphi_{M,i}^{\phi}$, respectively, where $\theta_{M,i}^{\phi} \coloneqq \theta_{M,0}^{\phi} + \Delta\theta_{M,i}^{\phi}$) still remain unknown in (16)–(18). Note that at the MV root bus, $\theta_{M,0}^{\phi}$ is simply set to zero without loss of generality, leading to $\theta_{M,i}^{\phi} = \Delta\theta_{M,i}^{\phi}$. Then, $\Delta\theta_{M,i}^{\phi}$ and $\mathbf{Z}_{M,i\text{-}j}$ should be estimated together by solving the optimization problem:

**$\mathbf{P}_3$: Line impedance estimation in the MV grid**

$$\min_{\mathbf{y}} \| \mathbf{g}(\mathbf{y}, \mathbf{u}) \|_2^2 , \tag{21}$$

where $$\mathbf{g}(\cdot) = \{\mathbf{g}_{i\text{-}j}(\mathbf{y})\}, \quad \forall (i,j) \in \mathcal{E}_M, \tag{22}$$

$$\mathbf{g}_{i\text{-}j}(\cdot) = \{[g_{i\text{-}j,r}^{\phi\mathrm{T}}, g_{i\text{-}j,x}^{\phi\mathrm{T}}]^{\mathrm{T}}\}, \quad \forall \phi \in \mathcal{P}_{ij}, \tag{23}$$

$$\mathbf{y} = [\mathbf{R}_M^{\mathrm{T}}, \mathbf{X}_M^{\mathrm{T}}, \Delta\boldsymbol{\theta}_M^{\mathrm{T}}]^{\mathrm{T}}, \tag{24}$$

$$\mathbf{u} = [|\mathbf{U}_M|^{\mathrm{T}}, |\mathbf{J}_M|^{\mathrm{T}}, \boldsymbol{\varphi}_M^{\mathrm{T}}]^{\mathrm{T}}. \tag{25}$$

As in $\mathbf{P}_1$, $g_{i\text{-}j,r}^{\phi}$ and $g_{i\text{-}j,x}^{\phi}$ in (22) and (23) represent the real and imaginary parts, respectively, of (1) for the line between MV buses $i$ and $j$. See (B1) and (B2) in Appendix B for more detailed expressions. In (24), $\mathbf{y}$ is the decision variable vector that contains the estimates of $\mathbf{R}_{M,i\text{-}j}$, $\mathbf{X}_{M,i\text{-}j}$, and $\Delta\boldsymbol{\theta}_{M,i}$ for the MV

© 2022 IEEE. Personal use is permitted, but republication/redistribution requires IEEE permission. See https://www.ieee.org/publications/rights/index.html for more information.
Authorized licensed use limited to: b-on: UNIVERSIDADE DO PORTO. Downloaded on August 07,2022 at 15:07:28 UTC from IEEE Xplore. Restrictions apply.

This article has been accepted for publication in IEEE Transactions on Power Delivery. This is the author's version which has not been fully edited and content may change prior to final publication. Citation information: DOI 10.1109/TPWRD.2022.3195075



lines and buses with all phases. Moreover, in (25), **u** is obtained from (16)–(20). In other words, the role of the calculated dataset $[|U^{\phi}_{M,i}|, |J^{\phi}_{M,i-j}|, \varphi^{\phi}_{M,i}]$ in $\mathbf{P_3}$ corresponds to that of the AMI dataset $[|V^{\phi}_{Li,n}|, |I^{\phi}_{Li,m\text{-}n}|, \varphi^{\phi}_{Li,n}]$ (or, equivalently, (6)) in $\mathbf{P_1}$. The GN algorithm is then applied to determine the optimal estimates of $\mathbf{Z}_{M,i\text{-}j}$ for all $i$ and $j$ that minimize the squared $L_2$-norm of $\mathbf{g}(\cdot)$ in (21).

Before applying the GN algorithm, $\mathbf{P_3}$ is extended to $\mathbf{P_4}$ using the time-series samples of **u**, as in the case of $\mathbf{P_1}$ and $\mathbf{P_2}$, as:

**$\mathbf{P_4}$: Extension of $\mathbf{P_3}$ for MV grid**

$$\min_{\tilde{\mathbf{y}}} \| \mathbf{G}(\tilde{\mathbf{y}}, \tilde{\mathbf{u}}) \|_2^2 , \tag{26}$$

$$\text{where } \mathbf{G}(\cdot) \coloneqq [\mathbf{g}(\cdot, \mathbf{u}_{(1)})^{\mathrm{T}}, \mathbf{g}(\cdot, \mathbf{u}_{(2)})^{\mathrm{T}}, \ldots, \mathbf{g}(\cdot, \mathbf{u}_{(K)})^{\mathrm{T}}]^{\mathrm{T}}, \tag{27}$$

$$\tilde{\mathbf{y}} \coloneqq [\mathbf{R}_M{}^{\mathrm{T}}, \mathbf{X}_M{}^{\mathrm{T}}, \Delta\tilde{\boldsymbol{\theta}}_M{}^{\mathrm{T}}]^{\mathrm{T}}, \tag{28}$$

$$\Delta\tilde{\boldsymbol{\theta}}_M \coloneqq [(\Delta\boldsymbol{\theta}_{M,(1)})^{\mathrm{T}}, (\Delta\boldsymbol{\theta}_{M,(2)})^{\mathrm{T}}, \ldots (\Delta\boldsymbol{\theta}_{M,(K)})^{\mathrm{T}}]^{\mathrm{T}}, \tag{29}$$

$$\tilde{\mathbf{u}} \coloneqq [\mathbf{u}_{(1)}{}^{\mathrm{T}}, \mathbf{u}_{(2)}{}^{\mathrm{T}}, \ldots \mathbf{u}_{(K)}{}^{\mathrm{T}}]^{\mathrm{T}}, \tag{30}$$

(24), and (25).

Table II shows the numbers of elements in (27) and (28) (i.e., the numbers of LIE equations and decision variables) for single-, double-, and three-phase lines between two MV buses. As discussed in Section III-C, the Jacobian matrix of $\mathbf{G}(\cdot)$ in (26) becomes full rank for $K \geq 4$, ensuring that the $\mathbf{P_4}$ solution is reliably obtained for any grid topology and line configuration.

TABLE II. NUMBERS OF EQUALITY CONSTRAINTS AND DECISION VARIABLES

| Line configuration | Number of elements in (27) | Number of elements in (28) |
|---|---|---|
| Single phase | $2K$ | $2 + K$ |
| Double phase | $4K$ | $6 + 2K$ |
| Three phase | $6K$ | $12 + 3K$ |

*D. Robust Estimation using Reinforcement Learning*

In practice, AMI datasets (i.e., $\mathbf{o}^{\phi}_i$ in (6)) are likely to include unknown measurement errors, which makes it impossible to solve the EIV problems $\mathbf{P_{1\text{–}4}}$ using standard WLS methods, as discussed in Section I. In the proposed strategy, an RL algorithm is integrated to compensate for measurement errors in the AMI datasets. The optimal adjustments $\Delta\mathbf{R}^{\phi}_{Li}$ and $\Delta\mathbf{X}^{\phi}_{Li}$ are then determined for the estimates of $\mathbf{R}^{\phi}_{Li}$ and $\mathbf{X}^{\phi}_{Li}$ (i.e., the $\mathbf{P_2}$ solutions), improving the accuracy and robustness of the LIE results for the LV grids and hence the MV grid. The RL-based error compensation is achieved using a deep deterministic policy gradient (DDPG) algorithm [30] where in each LV grid, an RL agent receives the AMI data samples (i.e., observation $\mathbf{o}^{\phi}_i$ in (6) or, equivalently, $\mathbf{o}^{\phi}_{i,(p)}$ in (11)) and interacts with the corresponding environment, as shown in Fig. 5. Typical Gaussian noise $v(p)$ is used for the exploration [31]. Note that different types of RL algorithms and exploration noise can also be adopted for the proposed error compensation.

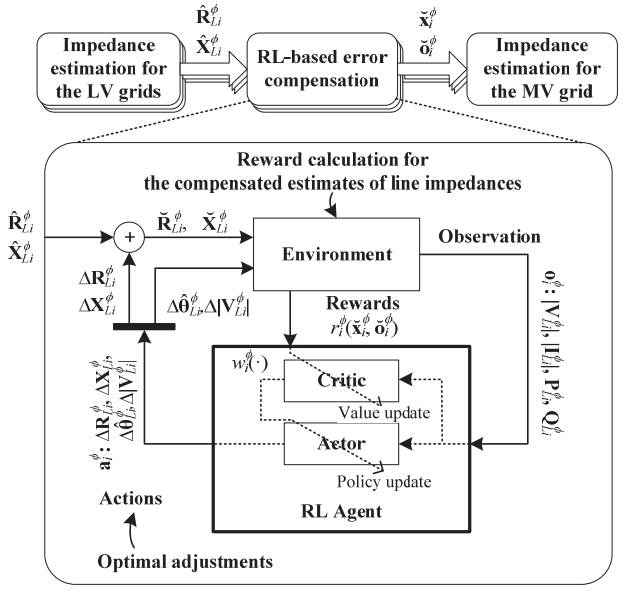


Fig. 5. Integration of the RL-based error compensation to the AMI-based LIE.

Specifically, the RL agent consists of an actor and critic, as shown in Fig. 5. The actor determines the optimal adjustments (i.e., action **a**), and the critic then calculates the Q function that represents the expectation value of the corresponding reward. For each RL agent, the action is defined as:

$$\begin{aligned}\mathbf{a}^{\phi}_i &\coloneqq \boldsymbol{\pi}^{\phi}_i(\mathbf{o}^{\phi}_i \mid \boldsymbol{\xi}^{\phi}_i) \\ &= [\Delta\mathbf{R}^{\phi}_{Li}{}^{\mathrm{T}}, \Delta\mathbf{X}^{\phi}_{Li}{}^{\mathrm{T}}, \Delta\hat{\boldsymbol{\theta}}^{\phi}_{Li}{}^{\mathrm{T}}, \Delta|\mathbf{V}^{\phi}_{Li}{}^{\mathrm{T}}|]^{\mathrm{T}},\end{aligned} \tag{31}$$

where $\boldsymbol{\xi}^{\phi}_i$ denotes the trainable weights of a neural network (NN) that models the policy $\boldsymbol{\pi}^{\phi}_i$, given $\mathbf{o}^{\phi}_i$. The action network represents a function of an AMI dataset $\mathbf{o}^{\phi}_i$. It provides the compensated estimate for each $\mathbf{o}^{\phi}_i$, implying that the action space does not change with the number of AMI datasets (i.e., $K$). After the policy $\boldsymbol{\pi}^{\phi}_i$ is trained, the Q function is then determined for $\mathbf{a}^{\phi}_i$ and $\mathbf{o}^{\phi}_i$ using a zero-discount factor, as:

$$v^{\phi}_i(\mathbf{o}^{\phi}_i, \mathbf{a}^{\phi}_i) = r^{\phi}_i(\mathbf{o}^{\phi}_i, \mathbf{a}^{\phi}_i). \tag{32}$$

This is because the LIE with measurement error compensation is inherently designed as a single-step RL problem. In other words, the action at the current state does not affect the next state. The Q function is then approximated using another NN $w^{\phi}_i(\mathbf{o}^{\phi}_i,\mathbf{a}^{\phi}_i \mid \boldsymbol{\zeta}^{\phi}_i)$ and trained to minimize the loss function $l$:

$$l(\boldsymbol{\zeta}^{\phi}_i) = (w^{\phi}_i(\mathbf{o}^{\phi}_i, \mathbf{a}^{\phi}_i \mid \boldsymbol{\zeta}^{\phi}_i) - z_t)^2, \tag{33}$$

where $z_t = r^{\phi}_i(\mathbf{o}^{\phi}_i, \mathbf{a}^{\phi}_i)$ is the target reward. Namely, $w^{\phi}_i(\mathbf{o}^{\phi}_i, \mathbf{a}^{\phi}_i \mid \boldsymbol{\zeta}^{\phi}_i)$ works as an approximate model of the reward $r^{\phi}_i(\mathbf{o}^{\phi}_i, \mathbf{a}^{\phi}_i)$, given the observations $\mathbf{o}^{\phi}_i$ and actions $\mathbf{a}^{\phi}_i$. It can be seen in (31)–(33) that $r^{\phi}_i(\mathbf{o}^{\phi}_i, \mathbf{a}^{\phi}_i)$ needs to be appropriately designed for the successful training of $\boldsymbol{\pi}^{\phi}_i(\mathbf{o}^{\phi}_i \mid \boldsymbol{\xi}^{\phi}_i)$ and $w^{\phi}_i(\mathbf{o}^{\phi}_i,\mathbf{a}^{\phi}_i \mid \boldsymbol{\zeta}^{\phi}_i)$ and, hence, the accurate compensation for the errors in the line impedance estimates. In this study, to incorporate the EIV model effectively, $r^{\phi}_i(\mathbf{o}^{\phi}_i, \mathbf{a}^{\phi}_i)$ is designed using the Geman-McClure (GM) loss function [32] with $l_1$-norm regularization [33], as follows:

$$r^{\phi}_i(\mathbf{o}^{\phi}_i, \mathbf{a}^{\phi}_i) = -\frac{\left\|\mathbf{f}^{\phi}_i(\breve{\mathbf{x}}^{\phi}_i, \breve{\mathbf{o}}^{\phi}_i)\right\|_2^2 + \lambda\left\|\boldsymbol{\beta}^{\phi}_i\right\|_1}{\mu + \left\|\mathbf{f}^{\phi}_i(\breve{\mathbf{x}}^{\phi}_i, \breve{\mathbf{o}}^{\phi}_i)\right\|_2^2 + \lambda\left\|\boldsymbol{\beta}^{\phi}_i\right\|_1}, \tag{34}$$

where

$$\breve{\mathbf{x}}^{\phi}_i = [\breve{\mathbf{R}}^{\phi}_{Li}{}^{\mathrm{T}}, \breve{\mathbf{X}}^{\phi}_{Li}{}^{\mathrm{T}}, \Delta\hat{\boldsymbol{\theta}}^{\phi}_{Li}{}^{\mathrm{T}}]^{\mathrm{T}}, \tag{35}$$

$$\breve{\mathbf{o}}^{\phi}_i = [\left|\mathbf{V}^{\phi}_{Li}\right|^{\mathrm{T}} + \Delta\left|\mathbf{V}^{\phi}_{Li}\right|^{\mathrm{T}}, \left|\mathbf{I}^{\phi}_{Li}\right|^{\mathrm{T}}, \boldsymbol{\varphi}^{\phi}_{Li}{}^{\mathrm{T}}]^{\mathrm{T}}, \tag{36}$$

$$\boldsymbol{\beta}^{\phi}_i = \Delta\left|\mathbf{V}^{\phi}_{Li}\right|, \tag{37}$$

$$\breve{\mathbf{R}}^{\phi}_{Li} = \mathrm{clip}(\hat{\mathbf{R}}^{\phi}_{Li} + \Delta\mathbf{R}^{\phi}_{Li}; \overline{\mathbf{R}}^{\phi}_{Li}, \underline{\mathbf{R}}^{\phi}_{Li}), \tag{38}$$

© 2022 IEEE. Personal use is permitted, but republication/redistribution requires IEEE permission. See https://www.ieee.org/publications/rights/index.html for more information.
Authorized licensed use limited to: b-on: UNIVERSIDADE DO PORTO. Downloaded on August 07,2022 at 15:07:28 UTC from IEEE Xplore. Restrictions apply.

This article has been accepted for publication in IEEE Transactions on Power Delivery. This is the author's version which has not been fully edited and content may change prior to final publication. Citation information: DOI 10.1109/TPWRD.2022.3195075



$$\check{\mathbf{X}}_{Li}^{\phi} = \text{clip}(\hat{\mathbf{X}}_{Li}^{\phi} + \Delta\mathbf{X}_{Li}^{\phi}; \bar{\mathbf{X}}_{Li}^{\phi}, \underline{\mathbf{X}}_{Li}^{\phi}). \quad (39)$$

In (34), $\|\mathbf{f}_i^{\phi}(\check{\mathbf{x}}_i^{\phi}, \check{\mathbf{o}}_i^{\phi})\|_2$ approaches zero and hence $r_i^{\phi}(\mathbf{o}_i^{\phi}, \mathbf{a}_i^{\phi})$ increases when the estimates of the line impedances and voltage angle differences become close to their actual values; please refer to (A6)–(A9) in Appendix A. Moreover, in (36), errors in voltage magnitudes are particularly considered, because the LIE results are more sensitive to errors in voltage measurements than to errors in power measurements, as discussed in Section IV-C. In (37), $\|\boldsymbol{\beta}^{\phi}{}_i\|_1$ is used to prevent an excessive large increase in the compensation for voltage magnitude errors. In (38) and (39), clip($\mathbf{x}$; $\bar{\mathbf{x}}$, $\underline{\mathbf{x}}$) limits the minimum and maximum values of $\Delta\mathbf{R}_{Li}^{\phi}$ and $\Delta\mathbf{X}_{Li}^{\phi}$, as:

$$\text{clip}(\mathbf{x}; \bar{\mathbf{x}}, \underline{\mathbf{x}}) = \begin{cases} \underline{x}(h), & \text{if } x(h) < \underline{x}(h), \\ x(h), & \text{if } \underline{x}(h) \le x(h) \le \bar{x}(h), \\ \bar{x}(h), & \text{if } x(h) > \bar{x}(h), \end{cases} \quad (40)$$

where $x(h)$ denotes the $h_{\text{th}}$ element in $\mathbf{x}$.

Given (34)–(39), the RL agent updates $\xi_i^{\phi}$ in (31) to minimize $l(\zeta_i^{\phi})$ in (33) using a gradient ascent algorithm, as:

$$\Delta\xi_i^{\phi}(\mathbf{o}_i^{\phi}, \mathbf{a}_i^{\phi}) = \nabla_{\mathbf{a}} v_i^{\phi}(\mathbf{o}_i^{\phi}, \mathbf{a}_i^{\phi}) \nabla_{\xi} \pi_i^{\phi}(\mathbf{o}_i^{\phi} \mid \xi_i^{\phi}), \quad (41)$$

while continuously monitoring $\mathbf{o}_i^{\phi}$. In other words, the RL agent learns the optimal $\boldsymbol{\pi}_i^{\phi}$ that maximizes $r_i^{\phi}$. After training, the RL agent instantaneously provides the optimal adjustments $\Delta\mathbf{R}_{Li(p)}^{\phi}$ and $\Delta\mathbf{X}_{Li(p)}^{\phi}$ for the AMI dataset $\mathbf{o}_{i(p)}^{\phi}$. In this paper, the average values of $\Delta\mathbf{R}_{Li(p)}^{\phi}$ and $\Delta\mathbf{X}_{Li(p)}^{\phi}$ for all $p$ are determined as $\Delta\mathbf{R}_{Li}^{\phi}$ and $\Delta\mathbf{X}_{Li}^{\phi}$, leading to $\check{\mathbf{R}}_{Li}^{\phi} = \mathbf{R}_{Li}^{\phi} + \Delta\mathbf{R}_{Li}^{\phi}$ and $\check{\mathbf{X}}_{Li}^{\phi} = \mathbf{X}_{Li}^{\phi} + \Delta\mathbf{X}_{Li}^{\phi}$. The RL agent also generates the compensated dataset $\check{\mathbf{o}}_i^{\phi}$ [i.e., (36)]. For the MV grid, $\check{\mathbf{R}}_{Li}^{\phi}$, $\check{\mathbf{X}}_{Li}^{\phi}$, and $\check{\mathbf{o}}_i^{\phi}$ are used in (16)–(20) and, consequently, $\mathbf{P_4}$ is established using the compensated estimates and datasets, as shown in Fig. 5. **Algorithm** shows the pseudo code to train the RL agent for LV grid $\mathcal{SN}(i, \phi)$.

**Algorithm:** Optimal adjustment with error compensation in $\mathcal{SN}(i, \phi)$

Initialize $\xi_i^{\phi}$ and $\zeta_i^{\phi}$ of the policy and Q networks.
Initialize the target networks $\bar{\bar{\boldsymbol{\pi}}}_i^{\phi}$ and $\bar{\bar{w}}_i^{\phi}$ by duplicating the weights of the actor and critic: $\bar{\bar{\xi}}_i^{\phi} \leftarrow \xi_i^{\phi}$ and $\bar{\bar{\zeta}}_i^{\phi} \leftarrow \zeta_i^{\phi}$.
Initialize the replay buffer [30].
**for** $ep = 1$ to $ep_{\max}$ **do**
  Receive initial observation $\mathbf{o}_{i,(1)}^{\phi}$ from AMI database.
  **for** $p = 1$ to $p_{\max}$ **do**
    Select action $\mathbf{a}_{i,(p)}^{\phi} = \boldsymbol{\pi}_i^{\phi}(\mathbf{o}_{i,(p)}^{\phi} \mid \xi_i^{\phi}) + v(p)$.
    Obtain $\Delta\mathbf{R}_{Li}^{\phi}$, $\Delta\mathbf{X}_{Li}^{\phi}$, $\Delta|\mathbf{V}_{Li}^{\phi}|$, and $\Delta\boldsymbol{\theta}_{Li}^{\phi}$ from $\mathbf{a}_{i,(p)}$.
    Calculate the reward $r_i^{\phi}(\mathbf{a}_{i,(p)}^{\phi}, \mathbf{o}_{i,(p)}^{\phi})$ using (34).
    Store the data $\mathbf{o}_{i,(p)}^{\phi}$, $\mathbf{a}_{i,(p)}^{\phi}$, and $r_i^{\phi}$ in the replay buffer.
    Sample mini-batches, each of which includes $N_b$ datasets.
    Update the critic with the mini-batch minimizing (33).
    Update the policy using the sampled policy gradient:
      $\xi_i^{\phi} \leftarrow \xi_i^{\phi} + 1/N_b \sum_k \Delta\xi_i^{\phi}(\mathbf{o}_{i,(k)}^{\phi}, \mathbf{a}_{i,(k)}^{\phi})$.
    Update the target networks $\bar{\bar{\boldsymbol{\pi}}}_i^{\phi}$ and $\bar{\bar{w}}_i^{\phi}$ by:
      $\bar{\bar{\xi}}_i^{\phi} \leftarrow \alpha\xi_i^{\phi} + (1-\alpha)\bar{\bar{\xi}}_i^{\phi}$,
      $\bar{\bar{\zeta}}_i^{\phi} \leftarrow \alpha\zeta_i^{\phi} + (1-\alpha)\bar{\bar{\zeta}}_i^{\phi}$.
    Receive next observation $\mathbf{o}_{i,(p+1)}^{\phi}$.
  **End**
**End**
Output $\check{\mathbf{R}}^{\phi}{}_{Li}$, $\check{\mathbf{X}}^{\phi}{}_{Li}$, and $\check{\mathbf{o}}^{\phi}{}_i$.

## IV. Simulation Case Studies

### A. Test System and Simulation Conditions

The proposed AMI-based LIE strategy was tested and compared with a conventional strategy using an LLS technique [15], [16], where (1) and (2) were linearly approximated. Table III (or, equivalently, a part of Table I) shows the main features of the proposed and conventional strategies. Specifically, comparative tests were conducted on an MV grid with single-, double-, or three-phase unbalanced lines, as shown in Fig. 6. The MV grid was implemented using the IEEE 37-node Test Feeder [34] with modifications based on [35] and [36]. It was connected to 32 single-phase LV grids, each of which included two to four end buses, thus resulting in a large-scale test bed.

TABLE III. Main Features of the Proposed and Conventional LIE

| Strategies | Network phases | Linear approximation | Problem solver | Data error compensation |
|---|---|---|---|---|
| Proposed | Unbalanced, multiple | - | GN | RL |
| Conventional | Unbalanced, multiple | O | LLS | LSF |

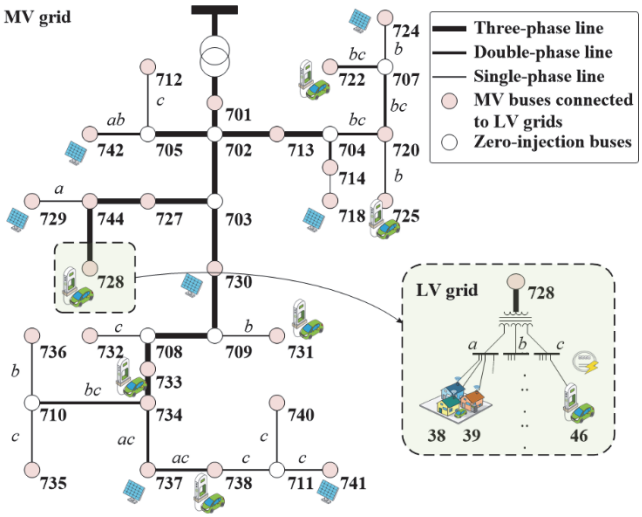


Fig. 6. Test system consisting of an MV grid, multiple LV grids, and DERs.

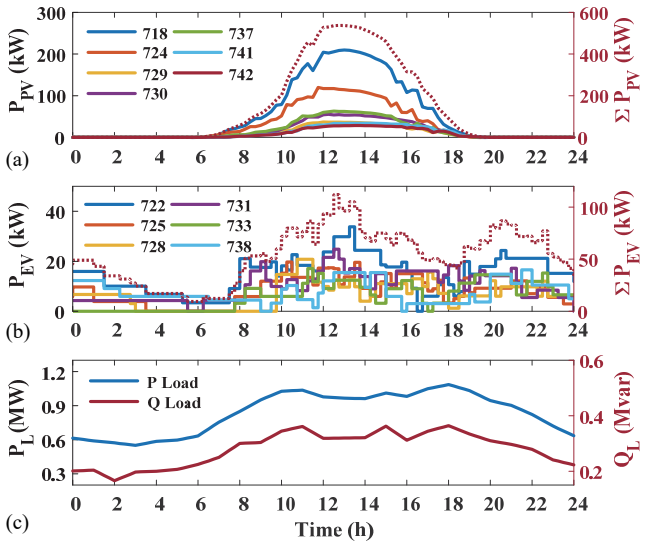


Fig. 7. An example of the 24-h profiles of (a) PV generation, (b) EV charging power, and (c) load demand in the test system.

© 2022 IEEE. Personal use is permitted, but republication/redistribution requires IEEE permission. See https://www.ieee.org/publications/rights/index.html for more information.
Authorized licensed use limited to: b-on: UNIVERSIDADE DO PORTO. Downloaded on August 07,2022 at 15:07:28 UTC from IEEE Xplore. Restrictions apply.

This article has been accepted for publication in IEEE Transactions on Power Delivery. This is the author's version which has not been fully edited and content may change prior to final publication. Citation information: DOI 10.1109/TPWRD.2022.3195075



TABLE IV. PARAMETER VALUES FOR THE CASE STUDIES

| Descriptions | Parameters | Values | Units |
|---|---|---|---|
| Initial line impedances | $Z^{\phi}_{Li}$, $\mathbf{Z}_{M,i\text{-}j}$ | 0, **0** | [pu] |
| Initial phase angle differences | $\Delta\boldsymbol{\theta}^{a}_{Li}(0)$, $\Delta\boldsymbol{\theta}^{b}_{Li}(0)$, $\Delta\boldsymbol{\theta}^{c}_{Li}(0)$, $\Delta\boldsymbol{\theta}^{a}_{Mi}(0)$, $\Delta\boldsymbol{\theta}^{b}_{Mi}(0)$, $\Delta\boldsymbol{\theta}^{c}_{Mi}(0)$ | 0, $-2\pi/3$, $2\pi/3$, 0, $-2\pi/3$, $2\pi/3$ | [rad] |
| Stop condition | $\varepsilon$ | $1\times10^{-10,}$ | |
| Learning rate | | $5\times10^{-5}$ | |
| Penalty factor for $l_1$-norm regularization | $\lambda$ | $1\times10^{-2}$ | |
| Scaling factor for GM loss function | $\mu$ | 0.1 | |
| Coefficient to update target networks | $\alpha$ | 0.2 | |
| Hidden layers and nodes | $L_\pi$, $L_Q$, $N_\pi$, $N_Q$ | 2, 2, 256, 256 | |
| Batch size | $N_b$ | 256 | |
| Maximum numbers of episodes and steps | $ep_{\max}$, $p_{\max}$ | $5\times10^{5}$, $10^{3}$ | |
| Maximum values of impedances and voltages | $\overline{\mathbf{R}}^{\phi}_{Li}$, $\overline{\mathbf{X}}^{\phi}_{Li}$, $\Delta\overline{\mathbf{R}}^{\phi}_{Li}$, $\Delta\overline{\mathbf{X}}^{\phi}_{Li}$, $\Delta\lvert\overline{\mathbf{V}}^{\phi}_{Li}\rvert$ | 0.15, 0.5, 0.1, 0.1, 0.02 | [pu] |
| Minimum values of impedances and voltages | $\underline{\mathbf{R}}^{\phi}_{Li}$, $\underline{\mathbf{X}}^{\phi}_{Li}$, $\Delta\underline{\mathbf{R}}^{\phi}_{Li}$, $\Delta\underline{\mathbf{X}}^{\phi}_{Li}$, $\Delta\lvert\underline{\mathbf{V}}^{\phi}_{Li}\rvert$ | 0.01, 0.05, –0.1, –0.1, –0.02 | [pu] |

The total number of resistance and reactance estimates to be determined was 240 for the MV lines and 178 for the LV lines. Appendix D provides the conductor parameters, configurations, and lengths of the LV lines [35], [36]. Fig. 6 shows that the test system also included seven and six MV buses to which photovoltaic (PV) arrays and electric vehicles (EV), respectively, were connected at the LV level. Fig. 7(a) and (b) represent the profiles of the total PV generation [41] and the total EV charging power [42], respectively, at each of the MV buses during an arbitrarily selected day between July 1, 2017 and August 22, 2017. Fig. 7(c) shows the profile of the total load demand during the same day [38].

In addition, Table IV lists the parameter values used for the case studies, particularly, with respect to the initial and stop conditions of the GN algorithm; the hyper- parameters of the RL agents; and the maximum and minimum limits for the LIE compensation. The stop condition parameter $\varepsilon$ was set to $10^{-10}$, considering the trade-off between the accuracy and time-efficiency of the LIE. Moreover, the RL hyper-parameters were chosen based on the discussion in [37]; note that other hyper-parameter selection methods still can be applied.

For the case studies, the real AMI datasets [$|\mathbf{V}^{\phi}_{Li}|$, $\mathbf{P}^{\phi}_{Li}$, $\mathbf{Q}^{\phi}_{Li}$] were collected every 15 minutes between July 1, 2017 and August 22, 2017 [38]. The size of the datasets was 5,000 with respect to time. The measurement errors $\mathbf{e}_{i,m}$ followed zero-mean Gaussian distributions with standard deviations $\boldsymbol{\sigma}_{i,m}$ [39]. The maximum error $\overline{\mathbf{e}}_{i,m}$ was set as 0.2% of the measurement of $|\mathbf{V}^{\phi}_{Li}|$, based on the 0.2-accuracy class meters of the ANSI C12.20 standard [40]. For $\mathbf{P}^{\phi}_{Li}$ and $\mathbf{Q}^{\phi}_{Li}$, $\overline{\mathbf{e}}_{i,m}$ were set to 1% of the corresponding measurements. In this study, $\boldsymbol{\sigma}_{i,m}$ was determined as $0.33\cdot\overline{\mathbf{e}}_{i,m}$ for a conservative evaluation of the performance of the proposed strategy under the condition of relatively large measurement errors. The performance was evaluated using the maximum absolute error (MAE) [14] as:

$$\text{MAE} = \max_i |x_i - \hat{x}_i|, \tag{42}$$

where $x_i$ and $\hat{x}_i$ are the actual and estimated values, respectively.

### *B. Accuracy and Convergence*

For the proposed and conventional strategies, the LIE results were obtained for an ideal case where the AMI datasets were collected without measurement errors. This enabled a fair comparison of the strategies, without requiring RL-based error compensation. Fig. 8 and Table V show that the proposed strategy led to significantly smaller errors in the LIE results for all MV and LV lines, compared to the conventional strategy. Note that the *y*-axis is represented in log scale. This confirmed that the proposed strategy exploited the AMI datasets more effectively and hence reflected the voltage variations along the MV and LV lines more accurately than the conventional strategy. This is mainly because in the proposed strategy, the nonlinear equations of the voltage drop between two interconnected nodes were directly used as the constraints for the optimal LIE problems (i.e., $\mathbf{P_2}$ and $\mathbf{P_4}$), whereas in the conventional strategy, the equations were linearly approximated with the assumption of no difference between the corresponding voltage phase angles. The comparisons shown in Fig. 9 also verify the improved accuracy of the proposed LIE strategy for different magnitudes of the total load demand in the

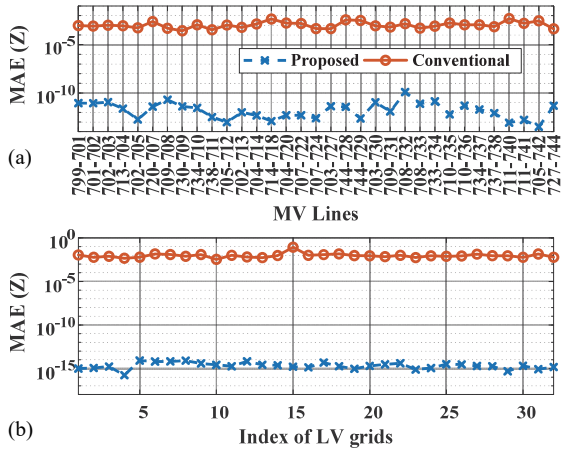


Fig. 8. Comparison of the MAEs for the line impedance estimates in the (a) MV and (b) LV grids.

TABLE V. MAES OF THE IMPEDANCE ESTIMATES OF THE MV AND LV GRIDS

| MAE | MV lines | | LV lines | |
|---|---|---|---|---|
| | R | X | R | X |
| Proposed | $5.64\times10^{-11}$ | $1.25\times10^{-10}$ | $4.16\times10^{-15}$ | $8.16\times10^{-15}$ |
| Conventional | $4.92\times10^{-3}$ | $3.19\times10^{-3}$ | $8.60\times10^{-2}$ | $1.11\times10^{-2}$ |

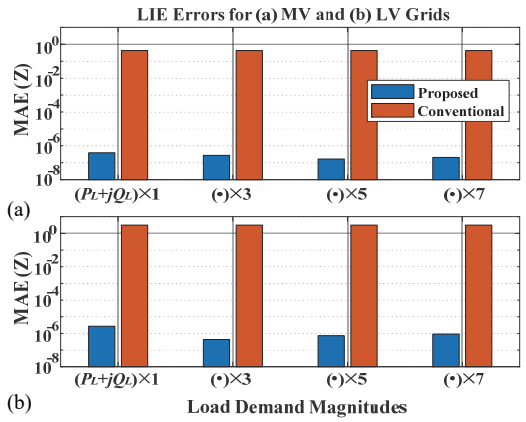


Fig. 9. Comparison of the MAEs for the line impedance estimates for different magnitudes of the total load demand $P_L+jQ_L$: (a) MV and (b) LV grids.

© 2022 IEEE. Personal use is permitted, but republication/redistribution requires IEEE permission. See https://www.ieee.org/publications/rights/index.html for more information.
Authorized licensed use limited to: b-on: UNIVERSIDADE DO PORTO. Downloaded on August 07,2022 at 15:07:28 UTC from IEEE Xplore. Restrictions apply.

This article has been accepted for publication in IEEE Transactions on Power Delivery. This is the author's version which has not been fully edited and content may change prior to final publication. Citation information: DOI 10.1109/TPWRD.2022.3195075



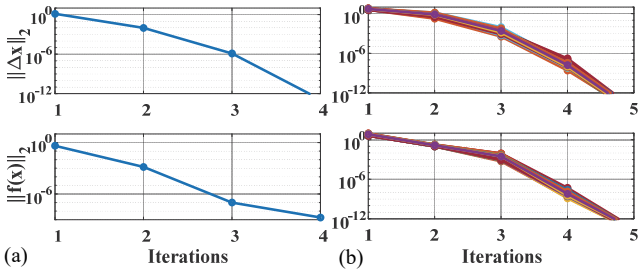


Fig. 10. Convergence of the GN iterations for the (a) MV and (b) LV grids.

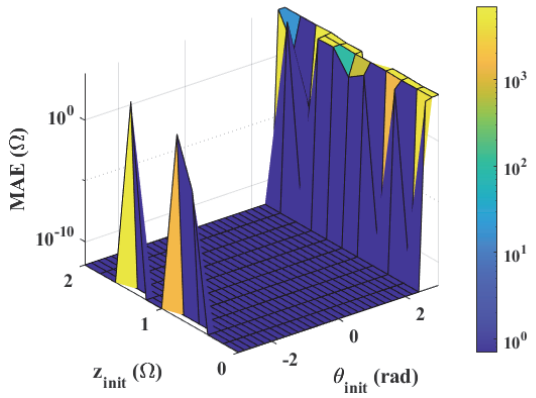


Fig. 11. Convergence of the GN iterations under various initial conditions.

test distribution grid.

In addition, Fig. 10 shows that only a few GN iterations were required for the convergence of the solutions to $\mathbf{P}_2$ and $\mathbf{P}_4$, ensuring the time efficiency of the proposed LIE strategy. The average computation times were 133.06 s and 4.19 s at the MV and LV levels, respectively, considering parallel LIE for the individual LV grids. Moreover, Fig. 11 shows that in general, the MAEs of the proposed LIE results remain low for different initial values of the line impedance estimates (i.e., before the first GN iteration), confirming the good convergence of the GN algorithm when applied to the optimal LIE problems with the nonlinear constraints on the voltage drop equations. This corresponds to the mathematical proof in Appendix C. It also verified that in practice, the proposed strategy can be successfully employed with various functions for distribution grid operation and monitoring.

### *C. Effects of Measurement Errors and Data Samples*

The sensitivity of the proposed LIE strategy was analyzed with respect to AMI measurement errors and the number of AMI dataset samples. Fig. 12 shows the MAEs for the MV grid and all the LV grids, when $\bar{\mathbf{e}}_{i,m}$ increased from 0.3% to 1.0% for both $\mathbf{P}^{\phi}_{Li}$ and $\mathbf{Q}^{\phi}_{Li}$ and from 0.01% to 1.0% for $|\mathbf{V}^{\phi}_{Li}|$. Note that the cases with $\bar{\mathbf{e}}_{i,m}$ > 0.2% do not satisfy the requirement for measurement accuracy in the ANSI standard, implying that the performance of the proposed strategy was conservatively evaluated with the practical, large level of measurement errors. It can be seen in Fig. 12 that an increase in $\bar{\mathbf{e}}_{i,m}$ for $\mathbf{P}^{\phi}_{Li}$ and $\mathbf{Q}^{\phi}_{Li}$ marginally affected the MAEs. However, as $\bar{\mathbf{e}}_{i,m}$ for $|\mathbf{V}^{\phi}_{Li}|$ increased, the MAEs gradually increased. This was also the case for the conventional strategy, demonstrating the need of the measurement error compensation for robust LIE.

In addition, Fig. 13 shows the variation in the MAEs for an increase in $K$. For the analysis, $\bar{\mathbf{e}}_{i,m}$ remained at 1% for $\mathbf{P}^{\phi}_{Li}$ and

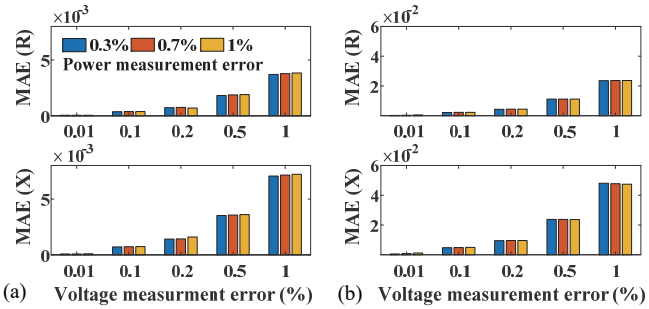


Fig. 12. MAEs of the line resistance and reactance estimates for variations in $\bar{\mathbf{e}}_{i,m}$ of the power and voltage measurements: (a) MV and (b) LV grids.

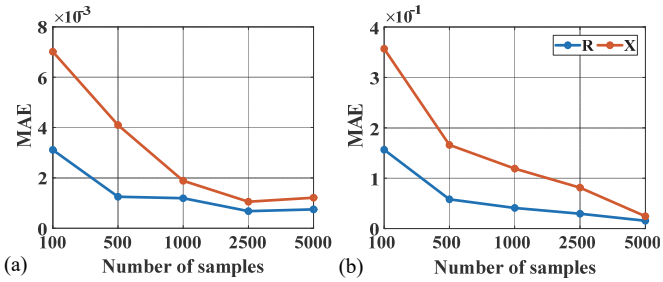


Fig. 13. MAEs of the line resistance and reactance estimates for variations in the number of the AMI dataset samples $K$: (a) MV and (b) LV grids.

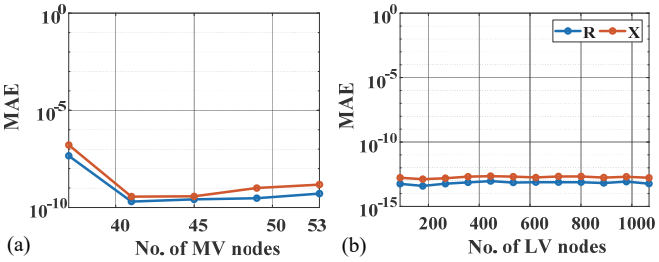


Fig. 14. MAEs of the line resistance and reactance estimates for variations in the number of nodes: (a) MV and (b) LV grids.

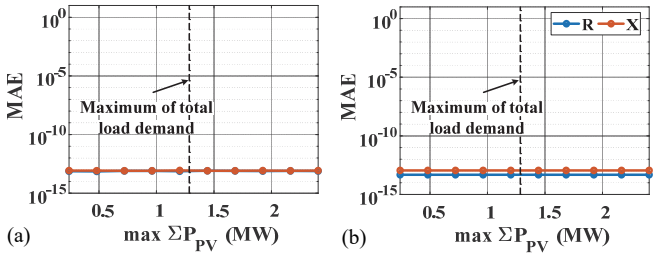


Fig. 15. MAEs of the line resistance and reactance estimates for variations in PV generation: (a) MV and (b) LV grids.

$\mathbf{Q}^{\phi}_{Li}$ and at 0.2% for $|\mathbf{V}^{\phi}_{Li}|$. As $K$ increased, the MAEs were gradually reduced to low levels. For $K$ = 5,000, the MAEs decreased by 75.9% and 82.7% for the MV grid and by 90.0% and 93.2% for the LV grids, compared to the case of $K$ = 100. This confirmed that the extension of the optimal LIE problems (i.e., from $\mathbf{P}_1$ and $\mathbf{P}_3$ to $\mathbf{P}_2$ and $\mathbf{P}_4$, respectively) was effective in exploiting a large number of AMI dataset samples for further improvement of the accuracy of the LIE results.

### *D. Effects of Grid Sizes and PV Generation*

The sensitivity of the proposed strategy was further analyzed with respect to the sizes of the MV and LV grids. Fig. 14(a) and 14(b) show the MAEs of the LIE results when the number of the MV nodes increased from 37 to 53 and the total number of the LV nodes rose from 89 to 1068, respectively. For such increases, additional nodes were inserted between two original

© 2022 IEEE. Personal use is permitted, but republication/redistribution requires IEEE permission. See https://www.ieee.org/publications/rights/index.html for more information.
Authorized licensed use limited to: b-on: UNIVERSIDADE DO PORTO. Downloaded on August 07,2022 at 15:07:28 UTC from IEEE Xplore. Restrictions apply.

This article has been accepted for publication in IEEE Transactions on Power Delivery. This is the author's version which has not been fully edited and content may change prior to final publication. Citation information: DOI 10.1109/TPWRD.2022.3195075



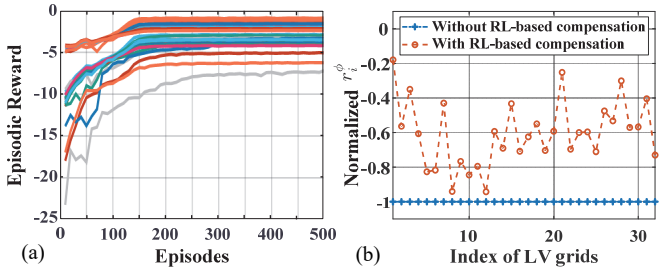


Fig. 16. (a) Convergence of episode rewards and (b) the normalized rewards of the LIE results for the cases with and without the RL-based error compensation.

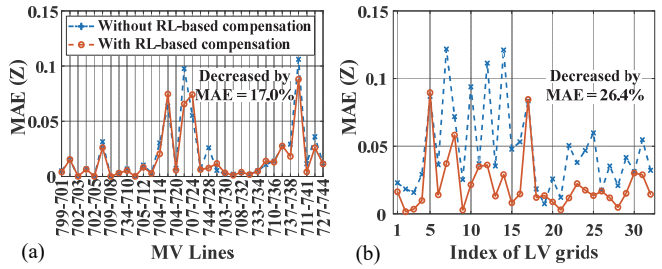


Fig. 17. MAEs of the line impedance estimates for the cases with and without the RL-based error compensation: (a) MV and (b) LV grids.

nodes, leading to the same configurations but shorter lengths of the distribution lines in the test system, shown in Fig. 6. It can be seen in Fig. 14 that for all the cases of the MV and LV grid sizes, the MAEs still remained low and were marginally affected, verifying the effectiveness and applicability of the proposed LIE strategy to larger-scale distribution systems.

The effect on the proposed strategy was also evaluated from different ratios of the PV penetration to the total load demand. Fig 15 shows the variations in the MAEs for an increase in the PV generation. As in Fig. 14, the MAEs remained low and were marginally influenced for all the cases of the PV generation; this is consistent with the results shown in Fig. 9. The sensitivity analysis results shown in Fig. 15 demonstrated the accuracy of the proposed LIE strategy even under the condition that the PV generation exceeds the total load demand and the reverse power flows occur in the distribution system.

### *E. Integration of RL-based Error Compensation*

The performance of the proposed strategy was further tested for cases with and without RL-based error compensation. For all $\mathbf{P}^{\phi}_{Li}$, $\mathbf{Q}^{\phi}_{Li}$, and $|\mathbf{V}^{\phi}_{Li}|$, $\bar{\mathbf{e}}_{i,m}$ were set to 1%, based on the sensitivity analysis in Section IV-C. Fig. 16(a) shows the average values of the rewards $r^{\phi}_{i}$ over episodes, which converged with small ranges of fluctuations after about 150 episodes for most of the RL agents and after approximately 450 episodes for all the agents. This confirmed that all the RL agents were successfully trained, leading to a considerable increase in the average rewards for the LV grids, as shown in Fig. 16(b). The RL agents were trained offline in parallel and then executed online. The average execution time of all the trained agents was $2.21\times10^{-4}$ s, demonstrating the scalability of the proposed RL-based error compensation algorithm. Note that in Fig. 16(b), the increased rewards differed for the individual LV grids, mainly due to the different topologies and random measurement errors.

Fig. 17 shows that with the RL-based error compensation, the MAEs of the line-impedance estimates in the MV and LV grids were further reduced by 17.0% and 26.4%, respectively, compared to those without compensation. Note that the *x*-axis in Fig. 17(a) is consistent with that in Fig. 8(a), although only alternating numbers are shown. The case study results confirm that the proposed RL-based compensation effectively improves the robustness of the proposed LIE strategy, particularly when applied to real distribution grids with noisy measurement data.

## V. Conclusions

This paper proposed a new AMI-based strategy to estimate line impedances in both MV and LV distribution grids. In the proposed strategy, hierarchical LIE was achieved by establishing lower- and upper-level optimization problems. The optimal LIE problems were formulated using local and global references to the voltage angles at the LV and MV levels, respectively, and extended for application of the AMI dataset samples collected over time. This enabled parallel LIE for individual LV grids and reliable acquisition of optimal line impedance estimates. For the problem formulation, the AMI datasets were collected only at the LV end-nodes, enabling the application of the proposed LIE strategy to different types of distribution grids with split, two, and three phases, for example. Moreover, unlike the conventional LLS technique, the problem formulation was achieved directly using the generalized, nonlinear equations of node voltage drops, improving the accuracy of the solutions (i.e., the LIE results). In addition, an RL-based method to compensate for measurement errors was developed and integrated with the hierarchical LIE, enhancing the robustness of the proposed strategy. The comparative case studies and sensitivity analyses were conducted on the test distribution system under various conditions, characterized mainly by the AMI dataset errors and numbers, the MV and LV grid sizes, and the load demand and PV generation. The distribution system was implemented using the IEEE test feeder with the real data of the AMI measurement, load demand, and PV generation. The corresponding results consistently demonstrated that the proposed LIE strategy significantly reduces the errors in the estimates of the all MV and LV line impedances than the conventional strategy for all the different conditions. The results also verified the scalability of the proposed strategy. Future research is still required, particularly, regarding the integration of the algorithms to estimate line capacitances and transformer impedances.

## References

[1] H. Bevrani, M. Watanabe, and Y. Mitani, *Power System Monitoring and Control*. Hoboken, NJ, USA: Wiley, Jun. 2014.

[2] N. Sockeel *et al.*, "Virtual inertia emulator-based model predictive control for grid frequency regulation considering high penetration of inverter-based energy storage system," *IEEE Trans. Sustain. Energy*, vol. 11, no. 4, pp. 2932–2939, Oct. 2020.

[3] J.-A. Jiang, J.-Z. Yang, Y.-H. Lin, C.-W. Liu, and J.-C. Ma, "An adaptive PMU based fault detection/location technique for transmission lines. I. Theory and algorithms," *IEEE Trans. Power Del.*, vol. 15, no. 2, pp. 486–493, Apr. 2000

[4] J.S. Kim, *et al.*, "A New Measure of Operating Speed and Consistency of Digital Protection Instruments Based on IEC 60255," IEEE Trans. Instrum. Meas., vol. 70, pp. 1-14, Oct. 2021.

[5] J.-A. Jiang, C.-W. Liu, and C.-S. Chen, "A novel adaptive PMU-based transmission-line relay-design and EMTP simulation results," *IEEE Trans. Power Del.*, vol. 17, no. 4, pp. 930–937, Oct. 2002.

[6] J. Peppanen, M. J. Reno, R. J. Broderick, and S. Grijalva, "Distribution system model calibration with big data from AMI and PV inverters," *IEEE Trans. Smart Grid*, vol. 7, no. 5, pp. 2497–2506, Sep. 2016.

© 2022 IEEE. Personal use is permitted, but republication/redistribution requires IEEE permission. See https://www.ieee.org/publications/rights/index.html for more information.
Authorized licensed use limited to: b-on: UNIVERSIDADE DO PORTO. Downloaded on August 07,2022 at 15:07:28 UTC from IEEE Xplore. Restrictions apply.

This article has been accepted for publication in IEEE Transactions on Power Delivery. This is the author's version which has not been fully edited and content may change prior to final publication. Citation information: DOI 10.1109/TPWRD.2022.3195075




[7] M. Lave *et al.*, "Distribution system parameter and topology estimation applied to resolve low-voltage circuits on three real distribution feeders," *IEEE Trans. Sustain. Energy*, vol. 10, no. 3, pp. 1585–1592, Jul. 2019.

[8] P. A. Pegoraro *et al.*, "Line impedance estimation based on synchrophasor measurements for power distribution systems," *IEEE Trans. Instrum. Meas.*, vol. 99, no. 4, pp. 1–2, Aug. 2018.

[9] J. Yu, Y. Weng, and R. Rajagopal, "PaToPaEM: A data-driven parameter and topology joint estimation framework for time varying system in distribution grids," *IEEE Trans. Power Syst.*, vol. 33, no. 4, pp. 4335–4347, May 2018.

[10] P. Shah and X. Zhao, "Network Identification using micro-PMU and Smart Meter Measurements," *IEEE Trans. Ind. Informat.*, early access

[11] M. Xiao *et al.*, "Distribution line parameter estimation driven by probabilistic data fusion of D-PMU and AMI,". *IET Gener. Transm. Distrib.* vol. 15, pp. 2883– 2892, Jun. 2021.

[12] A. Cooper and M. Shuster, "Electric company smart meter deployments: Foundation for a smart grid," The Edison Foundation, Washington, DC, USA, Tech. Rep., Dec. 2019.

[13] M. Manbachi and M. Ordonez, "AMI-based energy management for islanded AC/DC microgrids utilizing energy conservation and optimization," *IEEE Trans. Smart Grid*, vol. 10, no. 1, pp. 293-304, Jan. 2019.

[14] J. Zhang, Y. Wang, Y. Weng, and N. Zhang, "Topology identification and line parameter estimation for non-PMU distribution network: A numerical method," *IEEE Trans. Smart Grid*, vol. 11, no. 5, pp. 4440-4453, Sep. 2020.

[15] V. C. Cunha *et al.*, "Improving line parameter estimation using single-phase smart meter data," in *Proc. IEEE PESGM*, Jul. 2021, pp. 1-5

[16] V. C. Cunha *et al*., "Automated determination of topology and line parameters in low voltage systems using smart meters measurements," *IEEE Trans. Smart Grid*, vol. 11, no. 6, pp. 5028-5038, Nov. 2020.

[17] S. Han *et al.*, "An automated impedance estimation method in low-voltage distribution network for coordinated voltage regulation," *IEEE Trans. Smart Grid*, vol. 7, no. 2, pp. 1012–1020, Mar. 2016.

[18] W. H. Kersting, *Distribution System Modeling and Analysis*. Boca Raton, FL, USA: CRC Press, 2007.

[19] J. Peppanen, M. J. Reno, R. Broderick, and S. Grijalva, "Distribution system secondary circuit parameter estimation for model calibration," Sandia Nat. Lab., Albuquerque, NM, USA, Tech. Rep. SAND2015-7477, Sep. 2015.

[20] A. M. Prostejovsky *et al.*, "Distribution line parameter estimation under consideration of measurement tolerances," *IEEE Trans. Ind. Informat.*, vol. 12, no. 2, pp. 726–735, Apr. 2016.

[21] J. Zhang *et al.*, "A reinforcement learning based approach for on-line adaptive parameter extraction of photovoltaic array models," *Energy Convers. Manag.*, vol. 214, 112875, Jun. 2020.

[22] K. Xiong, C. Wei, and H. Zhang, "Q-learning for noise covariance adaptation in extended Kalman filter," *Asian J. Control*. pp. 1–14, 2020.

[23] B. Raeisy *et al.*, "Active methods to control periodic acoustic disturbances in-voking Q-learning techniques," *Nonlinear Dyn.,* vol. 74, pp. 1317–1330, 2013.

[24] *Electric Power Systems and Equipment—Voltage Ratings (60 Hertz)*, C84.1, American National Standards Institute (ANSI), 2020.

[25] M. Behnke *et al*., Secondary network distribution systems background and issues related to the interconnection of distributed resources, Technical Report NREL/TP-560-38079, July 2005

[26] M.W. Davis *et al.*, Modeling and verification of distributed generation and voltage regulation equipment for unbalanced distribution power systems, Subcontract Report NREL/SR-581-41885, July 2007

[27] M. I. Mossad, M. Azab and A. Abu-Siada, "Transformer Parameters Estimation From Nameplate Data Using Evolutionary Programming Techniques," *IEEE Trans. Power Del.*, vol. 29, no. 5, pp. 2118-2123, 2014

[28] H. Dirik, C. Gezegin and M. Özdemir, "A Novel Parameter Identification Method for Single-Phase Transformers by Using Real-Time Data," *IEEE Trans.Power Del.*, vol. 29, no. 3, pp. 1074-1082, Jun. 2014

[29] S. Boyd and L. Vandenberghe, *Convex Optimization*. Cambridge, U.K.: Cambridge Univ. Press, 2004.

[30] T. P. Lillicrap *et al.*, "Continuous control with deep reinforcement learning," in *Proc. Int. Conf. Learn. Representations*, Puerto Rico, 2016, page(s): 1–14.

[31] S. Fujimoto, H. van Hoof, and D. Meger, "Addressing function approximation error in actor-critic methods," in *Proc. 35th Int. Conf. Mach. Learn. (ICML)*, vol. 4, 2018, pp. 2587–2601.

[32] M. Black and A. Rangarajan, "On the unification of line processes, outlier rejection, and robust statistics with applications in early vision," *Int. J. Comput. Vis.*, vol. 19, pp. 57–92, July 1996.

[33] V. Kekatos *et al.*, "Distributed robust power system state estimation," *IEEE Trans. Power Syst.*, vol. 28, no. 2, pp. 1617–1626, May 2013.

[34] K. P. Schneider *et al.*, "Analytic considerations and design basis for the IEEE distribution test feeders," *IEEE Trans. Power Syst.*, vol. 33, no. 3, pp. 3181–3188, May 2018.

[35] T. Morstyn *et al.*, "Scalable energy management for low voltage microgrids using multi-agent storage system aggregation," *IEEE Trans. Power Syst.*, vol. 33, no. 2, pp. 1614–1623, Mar. 2018.

[36] K. Strunz *et al.*, "Developing benchmark models for low-voltage distribution feeders," in *IEEE Power Eng. Soc. Gen. Meet.*, Canada, Jul. 2009, page(s): 1–3.

[37] Y. J. Kim, "A Supervised-Learning-Based Strategy for Optimal Demand Response of an HVAC System in a Multi-Zone Office Building," *IEEE Trans. Smart Grid*, vol. 11, no. 5, pp. 4212-4226, Sep. 2020

[38] F. Bu *et al.*, "A timeseries distribution test system based on real utility data," 2019. [Online]. Available: https://arxiv.org/abs/1906.04078

[39] *IEEE Standard for Low-Frequency (less than 500 kHz) Narrowband Power Line Communications for Smart Grid Applications*, IEEE Std 1901.2-2013, Dec. 2013.

[40] *Electric Meters Code for Electricity Metering*, C12.1, American National Standards Institute (ANSI), 2008.

[41] S. Silwal *et al.*, "Open-source multi-year power generation, consumption, and storage data in a microgrid," *J. Renewable Sustain. Energy*, vol. 13, 025301, Mar. 2021.

[42] *Electric Vehicle Charging Station Usage (July 2011 - Dec 2017)·Open Data· City of Palo Alto*, Jan. 31, 2018. Accessed on: Jan. 25, 2021. [Online]. Available: https://data.cityofpaloalto.org/dataviews/244892/electric-vehicle-charging-station-usage-july-2011-dec-2017/

[43] Ferreira, Orizon Pereira, Max LN Gonçalves, and P. Roberto Oliveira. "Local convergence analysis of the Gauss–Newton method under a majorant condition." *J. Complexity*, vol. 27.1, pp. 111-125, 2011.


## APPENDIX

### *A. Formulation of* $\boldsymbol{P_1}$

For LV grid $\mathcal{SN}(i, \phi)$, (2) can be equivalently represented for the line voltage drop from bus $m$ to end bus $n \in \mathcal{LN}_i^{\phi}$, as:

$$\begin{aligned} V_{Li,m}^{\phi} - \left|V_{Li,n}^{\phi}\right| \exp(j\theta_{Li,n}^{\phi}) \\ = Z_{Li,m\text{-}n}^{\phi} \left|I_{Li,m\text{-}n}^{\phi}\right| \exp(j\theta_{Li,n}^{\phi} - j\varphi_{Li,n}^{\phi}), (m,n) \in \mathcal{LE}_i^{\phi}. \end{aligned} \tag{A1}$$

When bus $m$ has, at least, two downstream buses, (A1) can also be expressed as:

$$\begin{aligned} &\left|V_{Li,n}^{\phi}\right| \exp(j\Delta\theta_{Li,n}^{\phi}) - \left|V_{Li,l}^{\phi}\right| \exp(j\Delta\theta_{Li,l}^{\phi}) \\ &+ Z_{Li,m\text{-}n}^{\phi} \left|I_{Li,m\text{-}n}^{\phi}\right| \exp(j\Delta\theta_{Li,n}^{\phi} - j\varphi_{Li,n}^{\phi}) \\ &- Z_{Li,m\text{-}l}^{\phi} \left|I_{Li,m\text{-}l}^{\phi}\right| \exp(j\Delta\theta_{Li,l}^{\phi} - j\varphi_{Li,l}^{\phi}) = 0, \\ &\qquad (m,n),(m,l) \in \mathcal{LE}_i^{\phi}, \end{aligned} \tag{A2}$$

where $\Delta\theta_{Li,n}^{\phi} := \theta_{Li,n}^{\phi} - \theta_{Li,0}^{\phi}$. Moreover, for internal buses $o$ and $m$, (2) corresponds to:

$$V_{Li,o}^{\phi} - V_{Li,m}^{\phi} - Z_{Li,o\text{-}m}^{\phi} I_{Li,o\text{-}m}^{\phi} = 0, \quad (o,m) \in \mathcal{IE}_i^{\phi}, \tag{A3}$$

$$\begin{aligned} \text{where} \quad V_{Li,m}^{\phi} = \frac{1}{\left|\mathcal{LN}_{Li,m}^{\phi}\right|} \sum\nolimits_{g \in \mathcal{LN}_{Li,m}^{\phi}} \Big\{ \left|V_{Li,g}^{\phi}\right| \exp(j\theta_{Li,g}^{\phi}) \\ + Z_{Li,m\text{-}g}^{\phi} \left|I_{Li,m\text{-}g}^{\phi}\right| \exp(j\theta_{Li,g}^{\phi} - j\varphi_{Li,g}^{\phi}) \Big\}. \end{aligned} \tag{A4}$$

In (A3), $I_{Li,o\text{-}m}^{\phi}$ is equal to the sum of the currents injected into the end buses in the downstream of bus $m$, as:

$$I_{Li,o\text{-}m}^{\phi} = \sum_{p \in \mathcal{IN}_{i,m}^{\phi}} I_{Li,m\text{-}p}^{\phi} + \sum_{g \in \mathcal{LN}_{i,m}^{\phi}} |\, I_{Li,m\text{-}g}^{\phi} \,| \exp(j\Delta\theta_{Li,g}^{\phi} - j\varphi_{Li,g}^{\phi}), \tag{A5}$$

where $\mathcal{IN}_{i,m}^{\phi}$ and $\mathcal{LN}_{i,m}^{\phi}$ denote the sets of internal buses and end buses, for which the upstream buses include bus $m$. Note that in (A2)–(A5), $Z_{Li,m\text{-}n}^{\phi}$ and $\Delta\theta_{Li,n}^{\phi}$ are unknown. By arranging the left-side terms of (A2)–(A5) into the real and imaginary parts, the elements of $\mathbf{f}_i^{\phi}$ in the objective function of $\mathbf{P_1}$ can be defined as:

© 2022 IEEE. Personal use is permitted, but republication/redistribution requires IEEE permission. See https://www.ieee.org/publications/rights/index.html for more information.
Authorized licensed use limited to: b-on: UNIVERSIDADE DO PORTO. Downloaded on August 07,2022 at 15:07:28 UTC from IEEE Xplore. Restrictions apply.

This article has been accepted for publication in IEEE Transactions on Power Delivery. This is the author's version which has not been fully edited and content may change prior to final publication. Citation information: DOI 10.1109/TPWRD.2022.3195075



$$f_{i,1}^{\phi}(k) = \mathrm{Re}\Big\{|V_{Li,n}^{\phi}|\exp(j\Delta\theta_{Li,n}^{\phi}) - |V_{Li,l}^{\phi}|\exp(j\Delta\theta_{Li,l}^{\phi}) + Z_{Li,m\text{-}n}^{\phi}|I_{Li,m\text{-}n}^{\phi}|\exp(j\Delta\theta_{Li,n}^{\phi} - j\varphi_{Li,n}^{\phi}) - Z_{Li,m\text{-}l}^{\phi}|I_{Li,m\text{-}l}^{\phi}|\exp(j\Delta\theta_{Li,l}^{\phi} - j\varphi_{Li,l}^{\phi})\Big\}, \quad \text{(A6)}$$

$$f_{i,2}^{\phi}(k) = \mathrm{Im}\Big\{|V_{Li,n}^{\phi}|\exp(j\Delta\theta_{Li,n}^{\phi}) - |V_{Li,l}^{\phi}|\exp(j\Delta\theta_{Li,l}^{\phi}) + Z_{Li,m\text{-}n}^{\phi}|I_{Li,m\text{-}n}^{\phi}|\exp(j\Delta\theta_{Li,n}^{\phi} - j\varphi_{Li,n}^{\phi}) - Z_{Li,m\text{-}l}^{\phi}|I_{Li,m\text{-}l}^{\phi}|\exp(j\Delta\theta_{Li,l}^{\phi} - j\varphi_{Li,l}^{\phi})\Big\}, \quad \text{(A7)}$$

$$f_{i,3}^{\phi}(k) = \mathrm{Re}\left\{V_{Li,o}^{\phi} - V_{Li,m}^{\phi} + Z_{Li,o\text{-}m}^{\phi} I_{Li,o\text{-}m}^{\phi}\right\}, \quad \text{(A8)}$$

$$f_{i,4}^{\phi}(k) = \mathrm{Im}\left\{V_{Li,o}^{\phi} - V_{Li,m}^{\phi} + Z_{Li,o\text{-}m}^{\phi} I_{Li,o\text{-}m}^{\phi}\right\}, \quad \text{(A9)}$$

where $f_{i,1}^{\phi}(k)$, $f_{i,2}^{\phi}(k)$, $f_{i,3}^{\phi}(k)$, and $f_{i,4}^{\phi}(k)$ are the elements of the vector functions $\mathbf{f}_{i,1}^{\phi}$, $\mathbf{f}_{i,2}^{\phi}$, $\mathbf{f}_{i,3}^{\phi}$, and $\mathbf{f}_{i,4}^{\phi}$, respectively. Here, the number of elements of $\mathbf{f}_{i,1}^{\phi}$ (and $\mathbf{f}_{i,2}^{\phi}$) can be calculated as:

$$\sum_{m\in\mathcal{I}\mathcal{N}_i^{\phi}} |\mathcal{LE}_{i,m}^{\phi}|. \quad \text{(A10)}$$

Furthermore, the number of elements of $\mathbf{f}_{i,3}^{\phi}$ (and $\mathbf{f}_{i,4}^{\phi}$) can be calculated as $|\mathcal{IE}_i^{\phi}|$.

### *B. Formulation of $\boldsymbol{P_3}$*

For the MV line between two buses $i$ and $j$, (1) is divided into the real and imaginary parts and then expressed using (16)–(20), as:

$$g_{i\text{-}j,r}^{\phi} = \mathrm{Re}\{\, g_{i\text{-}j}^{\phi}\,\}, \quad g_{i\text{-}j,x}^{\phi} = \mathrm{Im}\{\, g_{i\text{-}j}^{\phi}\,\}, \quad \text{(B1)}$$

where

$$g_{i\text{-}j}^{\phi} = |U_{M,i}^{\phi}|\exp(j\Delta\theta_{M,i}^{\phi}) - |U_{M,j}^{\phi}|\exp(j\Delta\theta_{M,j}^{\phi}) - \sum_{\hat{\phi}\in\mathcal{P}_{ij}}\Big[Z_{M,i\text{-}j}^{\phi\hat{\phi}}\Big\{|J_{M,j}^{\hat{\phi}}|\exp(j\Delta\theta_{M,j}^{\hat{\phi}} - j\varphi_{M,j}^{\hat{\phi}}) + \sum_{k\in\mathcal{DN}_{Mj}^{\hat{\phi}}}|J_{M,k}^{\hat{\phi}}|\exp(j\Delta\theta_{M,k}^{\hat{\phi}} - j\varphi_{M,k}^{\hat{\phi}})\Big\}\Big]. \quad \text{(B2)}$$

This corresponds to the objective function of $\mathbf{P_3}$. In (B2), $\mathcal{DN}_{Mj}^{\phi}$ denotes the set of downstream buses for MV bus $j$ with phase $\phi$.

### *C. Convergence condition of GN algorithm*

We present the convergence condition of GN algorithm. Let us consider the following nonlinear least squares problem:

$$\min_{\mathrm{x}\in D} \frac{\mathbf{1}}{\mathbf{2}}\|\mathbf{f}(\mathbf{x})\|^{\mathbf{2}}, \quad \text{(C1)}$$

where $\mathcal{D}\subseteq\mathbb{R}^{\boldsymbol{n}}$ is an open set. As the solution of the nonlinear least square problem (C1) is rarely in closed form, many solution methods for the equation are iterative. Thus, (C1) can be solved using the following GN iterative procedure:

$$\mathbf{x}_{k+1} = \mathbf{x}_k - \left[\mathbf{J}^T(\mathbf{x}_k)\mathbf{J}(\mathbf{x}_k)\right]^{-1}\mathbf{J}(\mathbf{x}_k)\mathbf{f}(\mathbf{x}_k) \text{ for each } k \quad \text{(C2)}$$

The convergence of the GN method requires that $\mathbf{J}(\mathbf{x}_k)$ satisfies a Lipschitz condition. Namely, there exist $K > 0$ such that

$$\|\mathbf{J}(\mathbf{x}) - \mathbf{J}(\mathbf{y})\| \le K\|\mathbf{x} - \mathbf{y}\|, \forall \mathbf{x}, \mathbf{y} \in B(\mathbf{x}^*, r), \quad \text{(C3)}$$

where $B(\boldsymbol{a}, \delta) \coloneqq \{\mathbf{x} \in \mathcal{D}: \|\mathbf{x} - \boldsymbol{a}\| < \delta\}$ is an open ball at $a \in \mathcal{D}$ and radius $\delta > 0$; $\mathbf{x}^* \in \mathcal{D}$ denotes the (local) optimal point of the optimization problem (C1), and satisfies $\mathbf{f}(\mathbf{x}^*) = \mathbf{0}$. [43] provides the convergence region of (C1) under the Lipschitz condition of $\mathbf{J}(\mathbf{x}_k)$.

**Theorem 1**. [43] Let $\beta \coloneqq \left\|\left[\mathbf{J}^T(\mathbf{x}^*)\mathbf{J}(\mathbf{x}^*)\right]^{-1}\mathbf{J}(\mathbf{x}^*)\right\|$, $\kappa \coloneqq \sup\{t \in [0, R): B(\mathbf{x}^*, t) \in \mathcal{D}\}$, $r \coloneqq \min\{\kappa, 2/(3K\beta)\}$. Then the Gauss-Newton method for solving (C1), with initial point $\mathrm{x}_{\mathbf{0}} \in B(\mathbf{x}^*, \boldsymbol{t})/\{\mathbf{x}^*\}$ converges to $\mathrm{x}^*$. Moreover, if $2/(3K\beta) < \kappa$, then $r = 2/(3K\beta)$ is the best possible convergence radius.

In the proposed method $\mathbf{J}(\mathbf{x})$ satisfies the Lipschitz condition because all nonlinear functions in $\mathbf{J}(\mathbf{x})$ satisfy the Lipschitz condition, i.e., sine and cosine functions. Furthermore, $\beta$ in Theorem 1 is finite when we assume that we have sufficient AMI data because $\mathbf{J}^T(\mathbf{x}^*)\mathbf{J}(\mathbf{x}^*)$ is invertible and $\mathbf{J}(\mathbf{x})$ is finite for all $\mathbf{x} \in B(\boldsymbol{a}, \delta)$.

### *D. LV Lines in the Test System*

TABLE VI. LV LINE CONDUCTOR PARAMETERS

| Cable ID | $d_c$ (mm) | $R'_{ph}$ (Ω/km) | GMR (mm) |
|---|---|---|---|
| 1 | 27.19 | 0.3018 | 5.078 |
| 2 | 17.77 | 0.1509 | 5.078 |
| 3 | 24.89 | 0.6056 | 3.392 |

TABLE VII. LV LINE CONFIGURATIONS AND LENGTHS

| MV bus | LV buses | Phase | Cable ID | Cable length (ft.) | DER |
|---|---|---|---|---|---|
| 701 | 1, 2 | *a* | 1, 1 | 60, 73 | |
| | 3, 4 | *b* | 1, 1 | 53, 86 | |
| | 5, 6 | *c* | 2, 1 | 67, 87 | |
| 712 | 7–9 | *c* | 1, 1, 1 | 40, 82, 72 | |
| 713 | 10–12 | *c* | 1, 1, 1 | 74, 100, 87 | |
| 714 | 13–15 | *a* | 3, 3, 3 | 84, 62, 80 | |
| | 16–19 | *b* | 1, 1, 1 | 47, 62, 49, 66 | |
| 718 | 20, 21 | *a* | 1, 1 | 38, 93 | PV |
| 720 | 22–24 | *c* | 3, 3, 3 | 46, 90, 40 | |
| 722 | 25, 26 | *b* | 1, 1 | 42, 46 | EV |
| | 27, 28 | *c* | 2, 2 | 99, 38 | |
| 724 | 29, 30 | *b* | 1, 1 | 39, 94 | PV |
| 725 | 31–33 | *b* | 1, 1, 1 | 56, 97, 78 | EV |
| 727 | 34–37 | *c* | 3, 3, 2, 2 | 74, 84, 76, 45 | |
| 728 | 38–40 | *a* | 1, 3, 3 | 86, 44, 94 | |
| | 41–43 | *b* | 1, 2, 2 | 56, 97, 42 | |
| | 44–46 | *c* | 1, 1, 1 | 46, 91, 42 | EV |
| 729 | 47, 48 | *a* | 3, 3 | 46, 86 | PV |
| 730 | 49–51 | *c* | 2, 2, 2 | 91, 30, 34 | PV |
| 731 | 52–54 | *b* | 2, 1, 3 | 86, 76, 77 | EV |
| 732 | 55, 56 | *c* | 1, 2 | 54, 73 | |
| 733 | 57–59 | *a* | 1, 3, 2 | 34, 59, 96 | EV |
| 734 | 60–63 | *c* | 1, 1, 1, 3 | 94, 35, 71, 30 | |
| 735 | 64–66 | *c* | 3, 2, 2 | 46, 60, 84 | |
| 736 | 67–69 | *b* | 1, 3, 2 | 46, 43, 77 | |
| 737 | 70–72 | *a* | 1, 1, 2 | 92, 86, 44 | PV |
| 738 | 73–75 | *a* | 2, 3, 3 | 84, 39, 79 | EV |
| 740 | 76, 77 | *c* | 1, 1 | 90, 61 | |
| 741 | 78–80 | *c* | 1, 2, 2 | 48, 94, 42 | PV |
| 742 | 81–83 | *a* | 1, 1, 1 | 55, 90, 57 | PV |
| | 85–86 | *b* | 3, 3, 3 | 68, 43, 50 | |
| 744 | 87–89 | *a* | 2, 2, 2 | 34, 63, 57 | |

© 2022 IEEE. Personal use is permitted, but republication/redistribution requires IEEE permission. See https://www.ieee.org/publications/rights/index.html for more information.
Authorized licensed use limited to: b-on: UNIVERSIDADE DO PORTO. Downloaded on August 07,2022 at 15:07:28 UTC from IEEE Xplore. Restrictions apply.

This article has been accepted for publication in IEEE Transactions on Power Delivery. This is the author's version which has not been fully edited and content may change prior to final publication. Citation information: DOI 10.1109/TPWRD.2022.3195075



**Jaepil Ban** (Member, IEEE) received the Ph.D. degree in electrical engineering from Pohang University of Science and Technology, Pohang, South Korea, in 2020. From 2020 to August 2021, He was a postdoctoral researcher with Pohang University of Science and Technology, Pohang, South Korea.

Since 2021, he has been an Assistant Professor with Kumoh National Institute of Technology. His research interests include power system control, application of reinforcement learning, and state and line parameter estimation.

**Jae-Young Park** (Member, IEEE) received the B.S. degree (Hons.) in electrical engineering from Konkuk University, Seoul, South Korea, in 2015, and the Ph.D. degree in convergence IT engineering from the Pohang University of Science and Technology, Pohang, South Korea, in 2022. He is currently a Senior Researcher with Korea Institute of Energy Research, Daejeon, South Korea.

His research fields of interest include self-healing power systems, renewable energy resources, and grid-forming power converters.

**Young-Jin Kim** (Senior Member, IEEE) received the B.S. and M.S. degrees in electrical engineering from Seoul National University in 2007 and 2010, respectively, and the Ph.D. degree in electrical engineering from the Massachusetts Institute of Technology in 2015. He worked with Korea Electric Power Corporation as a Power Transmission and Distribution System Engineer from 2007 to 2011. He was also a Visiting Scholar with the Catalonia Institute for Energy Research in 2014, and a Postdoctoral Researcher with the Center for Energy, Environmental, and Economic Systems Analysis, Energy Systems Division, Argonne National Laboratory from 2015 to 2016.

He joined the faculty with the Pohang University of Science and Technology, where he is currently an Associate Professor with the Department of Electrical Engineering. His research fields of interest include distributed generators, renewable energy resources, and smart buildings.

**João P. S. Catalão** (Fellow, IEEE) received the M.Sc. degree from the Instituto Superior Técnico (IST), Lisbon, Portugal, in 2003, and the Ph.D. degree and Habilitation for Full Professor ("Agregação") from the University of Beira Interior (UBI), Covilha, Portugal, in 2007 and 2013, respectively.

Currently, he is a Professor at the Faculty of Engineering of the University of Porto (FEUP), Porto, Portugal, and Research Coordinator at INESC TEC. He was the Primary Coordinator of the EU-funded FP7 project SiNGULAR ("Smart and Sustainable Insular Electricity Grids Under Large-Scale Renewable Integration"), a 5.2-million-euro project involving 11 industry partners. His research interests include power system operations and planning, power system economics and electricity markets, distributed renewable generation, demand response, smart grid, and multi-energy carriers.

© 2022 IEEE. Personal use is permitted, but republication/redistribution requires IEEE permission. See https://www.ieee.org/publications/rights/index.html for more information.
Authorized licensed use limited to: b-on: UNIVERSIDADE DO PORTO. Downloaded on August 07,2022 at 15:07:28 UTC from IEEE Xplore. Restrictions apply.